LA-2909

LOS ALAMOS SCIENTIFIC LABORATORY
OF THE UNIVERSITY OF CALIFORNIA o LOS ALAMOS NEW MEXICO

A MONTE CARLO CALCULATION OF NEUTRON HEATING IN A NUCLEAR ROCKET PROPELLANT TANK

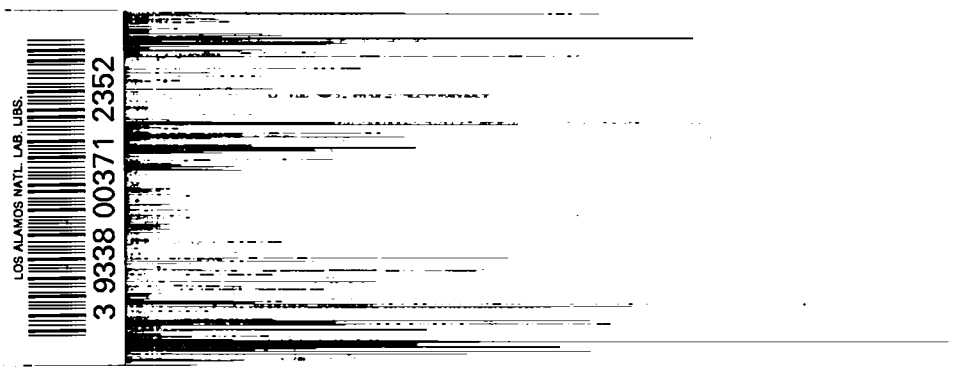

Printed in USA. Price $ 2.00. Available from the

Office of Technical Services
U. S. Department of Commerce
Washington 25, D. C.

LA-2909
UC-33, PROPULSION SYSTEMS AND
ENERGY CONVERSION
TID-4500 (21st Ed.)

LOS ALAMOS SCIENTIFIC LABORATORY
OF THE UNIVERSITY OF CALIFORNIA LOS ALAMOS NEW MEXICO

REPORT WRITTEN: April 30, 1963

REPORT DISTRIBUTED: September 16, 1963

A MONTE CARLO CALCULATION OF NEUTRON HEATING IN A NUCLEAR ROCKET PROPELLANT TANK

by

J. R. Streetman
G. A. Graves

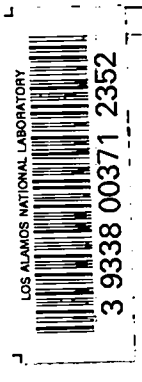

Contract W-7405-ENG. 36 with the U. S. Atomic Energy Commission

ABSTRACT

The calculation described here was undertaken to establish the principal features of neutron energy deposition, neutron migration, and neutron absorption within liquid hydrogen contained in the propellant tank of a nuclear rocket. Though the geometry was simplified in comparison to the probable complexity of any operational system, the results are readily generalizable and should assist considerably in understanding such systems.

The bulk of this report is concerned with the presentation and discussion of the neutron study, but the heating values found are compared, both in magnitude and in variation with propellant depth, to those expected from the scattering of gamma rays produced from neutron captures in liquid hydrogen and to those expected from the scattering of gamma rays coming from the reactor itself. An unshielded 1000 Mw reactor system is presumed.

ACKNOWLEDGEMENTS

It is a pleasure to acknowledge the invaluable help on this problem of C. J. Everett, E. D. Cashwell, and R. J. Schrandt, who handled its programming, coding, debugging, and operation.

CONTENTS

FIGURES

FIGURES (Continued)

FIGURES (Continued)

TABLES

TABLES (Continued)

TANK-REACTOR GEOMETRY, SOURCE USED, AND QUANTITIES PRINTED

This work deals with neutron propagation and heating within approximately the first 3 ft of liquid hydrogen (at density 0.07 g/cm^3) contained in a tank located 10 ft from the center of a reactor represented by a point source of neutrons (Figure 1).

The intensity of the point source was adjusted to provide about the same number of neutrons impinging per unit area on the tank bottom as one would expect from a properly oriented reactor centered on the source position - i.e., the "equivalent source" emission is ~0.6 neutron per reactor fission, or $\sim 1.98 \times 10^{19}$ neutrons per second per 1000 Mw, with the average energy of these ~0.8 Mev.

These flux data are based on DSN transport calculations of the axial leakage to be expected from typical reactor systems. Thus, the continuous curve of Figure 2 is a smooth representation of the high energy portion of the neutron leakage from an unshielded reactor of the type of interest to the nuclear rocket program, while the discretely stepped

line of that figure shows the spectrum which was used for the results reported here. These results are actually a combination and renormalization of some obtained in earlier unpublished work, wherein the effects from broad energy groups originally devised to fit a different spectrum were studied. The discrete approximation thus departs in detail from the continuous spectrum, but the departure is unimportant because the discrete spectrum was adjusted to have the proper energy content within each major energy group.

The source energy groups employed covered the range from 8 Mev to 17 kev, with the equivalent source intensities and energy content shown in Table I.

Two nearly equal areas were distinguished on the tank bottom, and a separate series of problems was run for each, mainly to determine whether neutrons striking the outer portion of the tank could contribute appreciably to the heating near the axis where the heating rate is highest. This information is needed to show whether tanks of other shape or diameter would exhibit the same maximum heating rates as those found in the present study. The distinguishing angle between the two problem series was approximately $\tan^{-1} 0.246$. This is seen in Figure 1 and in the more detailed view of the tank geometry presented in Figure 3, which also shows the energy deposition zones employed.

Nine "problems" were run for each of the two areas mentioned, each problem consisting of a set of histories sampled from a single group of the input energy intervals listed in Table I. All problems for Groups 1 and 2 followed 30,000 neutrons, whereas problems for Groups 3 to 6 each followed 20,000 neutrons. Three of the nine problems were partially redundant and their results are not reported here. They tested the effect of spectral modifications in the three groups of highest energy, and showed that a problem's results are more sensitive to its energy content than to moderate changes in its spectrum, thus indicating that spectral uncertainties should not be an appreciable concern in this study.

The twelve problems from which final results were obtained (six for each of the two areas of tank illumination) involved 280,000 histories altogether. They were separately normalized to 1000 Mw of power, via the appropriate energy contents shown in Table I, and printed singly and in various combinations so that their results could be examined individually and in composite.

The detailed geometry used is shown in cross section in Figure 3. The size of the sampling boxes increased as a function of depth into the tank so as to provide detail where the statistics were good and as much information as

practicable further into the tank where fewer neutrons were expected. The neutrons were followed until they escaped from the tank or until their energy dropped below 10 kev.

For each sampling box, five quantities were accumulated: the energy deposited by all neutron scatters, the energy deposited by first collisions only, the number of neutrons whose histories were terminated ("cut") by virtue of their post-collision energies having fallen below 10 kev, the total energy possessed by neutrons cut in the box, and a sum of the total energy deposited by neutron scatters plus that deposited by history terminations. The treatment of terminated neutrons will be discussed later.

The number of neutrons escaping the tank was accumulated in 10 energy groups for the front and back faces and for 5 conical surface areas denoted by the boundary lines on the side of the tank in Figure 3. For two internal test planes (shown dotted in Figure 3), the number of neutrons crossing in each direction was also accumulated as a function of energy.

The reasonable assumption was made that the sole interaction between energetic neutrons and hydrogen atoms is elastic scattering, a process which is isotropic in the center-of-mass system. The cross sections used for this process were the total hydrogen atom cross sections of

BNL-325.[1] They and their corresponding mean free paths are tabulated in the Appendix to this report, along with brief comments on the scattering law.

RESULTS

Energy Deposition

Figure 4 presents values for the total power generated by neutrons within the segments of propellant along the axis of the tank. The straight line which has been drawn through the early portion of the data shows that the energy deposition drops off for about 2 ft at a nearly constant factor of 10 per foot, as if there were an effective mean free path (e-folding) for energy absorption of ~13 cm.

This near constancy in the net attenuation factor is striking, in view of the large variation in monoergic attenuation factors within the neutron energy range, and must be a consequence of the shape and broad energy distribution of the input spectrum. Since most reactor leakage spectra are likely to be of somewhat similar shape in their energy-carrying region, with a monotonic increase in neutron number from high to low energies, this result probably has a rather general validity. Thus, it should be possible to obtain useful first estimates of the heating from any reactor

source by presuming a factor of 10 per foot fall off in the energy deposition from that in the region of incidence. The latter can always be calculated quite readily for any spectrum from first collision energy losses alone.

The heating beyond the 2 ft depth appears to be greater than that which would be predicted by an extrapolation from this initial rate of change (the statistics are not adequate to support this conclusion unambiguously), but most of the energy from the source is already accounted for before this region of low deposition is reached.

In Figure 5 the total energy deposition rates just discussed are compared to those from first collisions alone and to the rates at which energy is carried below the 10 kev cutoff limit, all being expressed for the axial segments as a function of depth in the tank. The numerical values, in ergs per second per gram of propellant,* corresponding to points on the figure, are compiled (along with other information) in Table II.

From the figure, it can be seen that the neutrons did not carry enough energy at cutoff to affect the validity of the deposition results. (Since this cutoff energy ultimately would have been deposited by elastic scattering, its

---

*10^7 erg/gm-sec = 1 w/gm $\simeq$ 0.43 BTU/lb-sec $\simeq$ 0.24 cal/gm-sec

value has been collected into the total in this report whenever terms like "total power," "total scattering," etc., are used.)

First collisions necessarily account for nearly half of the energy deposited in the entire propellant volume considered, but their percentage importance in local heating varies with propellant depth, as one can see in Figure 5. At the face of the tank the energy deposited is nearly all due to first collisions, but, with increasing depth (to at least 50 cm) more and more of the energy deposited is due to scattered neutrons. Beyond 50 cm it is impossible to say whether the two curves continue to diverge, though at some large distance they should become parallel, because the ultimately controlling source is the more-readily-penetrating high-energy component of the incident spectrum. Beyond 50 cm depth, it appears that first collisions account for only some 20 percent of the total neutron energy deposited. Similar results should be obtained for almost any other input spectrum.

Figure 5 and several of the succeeding figures are taken directly from the SC 4020 output of the computer. In them it can be noted that the statistics of the Monte Carlo are quite good. Though this might have been expected, since the data are based on 280,000 neutron histories, the fact

that the results lie close to a smooth curve is one of the better indications of the adequacy of the sample.

The variation of deposited energy with radial segment number may be seen in Figure 6, whose data are given in Table III. (The plotting numbers defining curves in the figure represent the order of radial segments counting from the axis of the tank.) Notice that the energy deposited is almost independent of radial position, though the outer segments absorb slightly, but progressively, less energy. Radial segment 7 energy deposition drops below the others for a time, but this may be explained by noting the favorable possibility afforded in it for scatter out of the tank (cf. Figure 3 to review the relative configuration of the various radial segments). This explanation is supported by the fact that the "7" curve rejoins the others as an eighth segment, added outside at 40 cm depth, becomes thicker. (Segment 8 data were omitted in order to avoid further complication of the figures.)

The total energy deposition from the separate spectral groups 1 through 6 is shown as a function of depth and radius in Figures 7 through 12 and given in Tables IV through IX. The energy limits of the six groups are those previously given in Table I. The penetration of the various groups is about as would be expected from the energy, though one

should note that the effective mean free paths for energy absorption exceed the collision mean free paths of the incident neutrons. This is shown in Figure 13, where these λ_{eff}'s (as deduced from Figures 7 through 12) are compared with the collision mean free path used in the input to this program. Since the energy-absorption curves for the individual groups depart appreciably from a straight line (unlike the composite curve in Figure 4 for the total energy deposited), the values of λ_{eff} in Figure 13 are not well defined. Except for the highest energy group, however, each tends to be longer than the largest collision mean free path for any of the incident neutrons within the group, thus indicating the role played by multiple collisions in sustaining the heating in depth.

Figure 14 shows the relative importance of the various source groups to the total energy deposition at various depths in the propellant near the tank axis. Though the highest energy group contains only about 20 percent of the incident energy, it accounts for more than 80 percent of the energy deposition at 2 ft and for all practical purposes is the only group that needs consideration at 3 ft.

Figures 15 and 16 show clearly that neutrons do not deposit much energy in any part of the propellant that is not near their original undeflected path. We will refer to

"inner" neutrons as those whose incident angle from the axis of the tank was less than $\tan^{-1}$ 0.246 and to the others as "outer" neutrons. From the geometry (cf. Figure 1 or Figure 3) one sees that, near the face of the tank, inner neutrons mainly "illuminate" radial segments 1 through 4, while segments 5 through 7 are illuminated mainly by outer neutrons. Accordingly, at small penetrations, Figure 15 (for inner neutrons) shows large heat input to segments 1 through 4 and very little heat input to segments 5 through 7, while Figure 16 (for outer neutrons) shows the converse. Even at greater depths, significant heating occurs only in illuminated areas. For example, segment 5 is increasingly illuminated by inner neutrons with increasing depth into the tank, and its heating values move up to join the other curves of Figure 15 in rough proportion to this illumination. Correspondingly, Figure 16 shows curve 5 dropping away from the others with increasing depth as the fifth segment becomes less well illuminated by the outer neutrons. (In Figures 15 and 16, the SC 4020 output of the computer has been allowed to follow its normal practice of placing points at the edge of the graph which really belong off-scale. Regardless of the appearance this creates, there is no depth at which the heating in the nonilluminated regions approaches that in the illuminated regions, as can be verified by consulting Tables

X and XI, which list the data of these figures.)

In particular, one should observe from these two figures that the heating at any depth in radial zone 1 is determined solely by the neutrons emitted within the inner solid angle and striking near the axis of the tank. Thus, it can be concluded that the heating rates in the inner part of the tank, where the heat input is highest, are quite insensitive to tank diameter, so that the values reported here should have applicability to tanks of any diameter.

Leakage and Transmission

About 5 percent of the neutrons striking the tank were found to escape through the side or faces. These neutrons carried away some 2 percent of the incident energy. Detailed data on the space distribution of the neutron number losses and energy losses from the individual groups, as well as for the total problem, are given in Tables XII and XIII.

Figure 17 shows the incident neutron spectrum collected into 10 energy intervals for comparison against the ten-group appearance of the neutrons which cross planes at 8, 20, and 92 cm in the direction of increasing depth. The data appear in the proper relative intensity. So few neutrons are transmitted through the entire 92 cm of liquid that the statistics for this plane are fairly poor. However, the change in the spectral quality of the transmitted radiation to a predomi-

nantly high energy distribution ("hard" spectrum) is clearly shown.

Bearing in mind the fact that the flux at the back face would be less than that at the front face by a factor of ~1.7 even without the hydrogen (due to distance effects alone), this curve also shows that even the most penetrating group of higher energy neutrons would be attenuated by a factor of ~430 by 92 cm of LH_2, while other data show that the reactor's total number current (including thermals) would be reduced by ~1800 in the same distance. The total decrease in transmitted energy from these 3 ft of hydrogen (with distance correction applied) is ~515. It is obvious that at least this degree of neutron shielding is available for protecting a payload whenever the depth of propellant intervening between it and the reactor equals or exceeds 3 ft, which would be most (and could be all) of the time that the reactor is in operation.

The difference in character between the transmitted spectra and the reflected or back-scattered spectra may be seen by comparing Figures 17 and 18. The latter figure shows the energy distribution of the neutrons crossing planes at 0, 8, and 20 cm depth in the direction of the reactor. The spectrum is quite depleted at high energies - e.g., no neutrons were returned through the entrance face of the tank

with energies above 1.4 Mev.

The individual group calculations provide some insight into the reflection of neutrons as a function of energy. Figure 19 gives the ratio of the number of neutrons crossing each test plane in the backward direction to the number crossing it in the original (incident) direction. The ratio of the energy returning across each plane to the energy crossing it in the original direction is also plotted. These data, expressing the fractional reflection of number or energy, are shown as a function of the average energy of the neutrons crossing the planes in the inward direction. One would expect a low percentage return in number or energy from the tank face (0 cm), since neutrons strike it almost perpendicularly and thus can hardly escape in one collision because of the 90° limitation imposed by the scattering law (cf. Appendix). The test planes at 8 and 20 cm depth are crossed by a more diffuse flux which should (and does) exhibit a higher reflection probability. The evidence is that only $\sim$2 percent of the neutrons and $\sim$0.1 percent of the energy are returned for the near-normal incidence at the entering plane, and only $\sim$5 percent of the neutrons and $\sim$0.5 percent of the energy are returned for the more diffuse incidence. It should be borne in mind, however, that the neutrons whose motions are described here were all above the

10 kev cutoff energy and that these results, particularly for number reflection, are sensitive to the cutoff energy. This has undoubtedly influenced the small neutron and energy return shown in Figure 19 from the group whose average energy at incidence was nearest cutoff. The study of number and energy albedo is interesting, but it will not be pursued further here since excellent information on this (and many other points) is available in a report[2] written by M. O. Burrell of the Marshall Space Flight Center.*

Cutoffs and the Capture Distribution

In the calculation which we have been describing, a neutron's history was terminated either on escape from the tank or on attaining a post-collision energy below 10 kev. Since there were relatively few escapes, most neutrons followed a sequence of energy-degrading collisions to cut-off, so that the main determinant of the number of collisions experienced in a given problem was the initial energy of the group neutrons.

---

*Burrell used Monte Carlo techniques to investigate the effect of monoergic sources impinging at various angles of incidence on either cylindrical or slab geometries of liquid hydrogen. Thus his results are somewhat complementary to those from the distributed-spectrum integral-geometry approach of the present work and should receive the attention of anyone seeking a broader understanding of radiation propagation in LH_2. In general, all applicable comparisons indicate good agreement between the neutron behavior revealed in that study and in this.

This can be seen in Table XIV, which summarizes the collision data both on the neutrons which underwent cutoff and on those which escaped. (For the fullest understanding of neutron leakage behavior, one should supplement the data in Table XIV with that in Tables XII and XIII.)

The average character of neutrons remaining in the tank and scattering to cutoff energies is influenced by the character of those which leak out. This fact can be used to explain the small, but consistent, difference in the average number of collisions to cutoff observed between the "inner" and "outer" problems in Table XIV. More high energy leakage occurred for neutrons incident on the outer portion of the tank. Back-scattering, with its attendant energy degradation, was not required to effect escape from these regions, and many of the energetic (long mean free path) neutrons apparently were able to reach the tank boundary after one or even several small-angle low-energy-loss scatters. Consequently a larger percentage of low energy neutrons were left behind in "outer" problems (since the scattered neutrons distribute uniformly in energy from initial energy to zero energy) than in those of "inner" incidence, and these residual lower energy neutrons should and did exhibit a slightly lower average number of collisions to cutoff.

The total number of neutrons "cut" from all groups per cubic centimeter per second is shown for seven radial segments as a function of distance into the tank in Figure 20. The number cut is nearly independent of radial position, except for the understandable deviation of curve 7 where leakage has influenced the result. Figures 21 through 26 show this cutoff data group by group.

These cutoff distributions have been used as capture distributions, in order to be able to calculate a capture gamma dose rate, on the assumption that neutrons of energy below 10 kev can not migrate very far. Several points support this usage, but since the subject has sometimes been misunderstood, the reasoning is discussed below.

First, the scattering mean free path of these neutrons is already less than 1.3 cm at cutoff (based on a scattering cross section of 18 barns per atom) and decreases to around 1.1 cm during the approach to thermal energies. With so many closely spaced, direction-randomizing collisions, it would appear to be difficult for neutrons to go far during this thermalization process.*

---

*This is supported by the calculation of Burrell, op.cit.,[2] in which neutrons were followed to post-collision energies below 1 ev (4 decades lower in energy than in this calculation), but the space distributions of cutoffs obtained were quite similar to those of the present calculation for similar incident energies.

Second, it is true that the scattering probability changes whenever neutron energies become comparable to the binding energy between the two atoms of the hydrogen molecule, but the absorption probability is not subject to change by interference effects, going as 1/V for all hydrogen molecules, independent of their type. Because of this scattering cross-section change, parahydrogen (the major equilibrium constituent of liquid hydrogen) has a considerably lower total cross section at low energies than does orthohydrogen. However, the minimum parahydrogen cross section (at 0.010 ev) is still ~3 barns,[3] yielding a maximum collision mean free path under 8 cm for all neutrons in the low energy region. When such facts are considered, 8 cm has been estimated as a reasonable upper limit* to the average migration distance before absorption of neutrons below 10 kev in pure parahydrogen.

This would be a completely inconsequential source displacement for the purposes of calculating capture gamma heating at any appreciable distance. The mean free paths in liquid hydrogen are so large for the 2.23 Mev neutron-capture gamma rays (the collision mean free path is ~172 cm and the energy-absorption mean free path is ~315 cm) that the total

---

*The writers are indebted to Gordon Hansen of this Laboratory for a helpful discussion in this connection.

energy deposition within the tank can hardly be affected by such small variations in the capture point.

While they can have little effect on the total energy absorption in the tank, deviations in the distribution of neutron absorptions (i.e., the capture source) do affect the intensity of local heating. However, further diffusion of neutrons between the attainment of cutoff and the actual capture would serve only to reduce the maximum in the capture distribution we advance below. Such a change would reduce both the maximum capture heating and the steepness of the local energy absorption gradient and thus decrease the severity of the fluid circulation problems to be predicted from such gradients -- for example, when the density gradients arising from nonuniform fluid heating are reduced, the chances of convective circulation or propellant stratification under the action of these buoyancy forces diminish. For such reasons, we feel that employing cutoff distributions for capture distributions is not only adequate, but it is also conservative.

To get the final capture distribution resulting from all the reactor neutron leakage, the data of Figure 20 first had to be modified to allow for neutrons which were not run in the Monte Carlo because of their low energy content, but which would still produce capture gammas. These neutrons

were assumed to produce the same capture distribution as the lowest energy group of the Monte Carlo. Their inclusion gives the postulated total axial capture distribution of Figure 27 and Table XV. Nearly 80 percent of these captures occur in the first 10 cm of propellant and over 90 percent occur in the first 30 cm.

In order to use an existing computer code to generate heating values from this volume-distributed capture source, it was represented by fourteen source planes located at propellant depths of 1, 3, 5, 7, 9, 12, 16, 20, 24, 28, 35, 45, 55, and 65 cm. The on-axis gamma generation rate appropriate to each plane was determined through Figure 27, and the capture intensity at any other position on the plane was related to this axial value by an inverse square ratio on the distance of the two points from the reactor center. (Cross-checks showed that the deviations from the correct capture distribution in this approximation were usually less than the statistical uncertainty in the "correct" values, and certainly unimportant to the total heating.) The heating calculation presumed that the gammas emanated uniformly from each capture site; the flux to the detector point was diminished by square-law factors as well as by attenuation from Compton scattering, photoelectric absorption, and pair production; and a buildup correction was used to allow for

multiple scatters. The dose (heating) was integrated over the source in each plane, and was then summed for all planes to give the total heating from capture gammas at each of the on-axis points studied. These results are presented in the next chapter.

COMPARISON OF NEUTRON HEATING WITH OTHER MAJOR RADIATION SOURCES

Figure 28 compares the propellant energy input rates to be expected at various depths along the axis of this tank from each radiation cause, and totals the effects from all radiation sources. All the data are normalized for a 1000 Mw unshielded reactor source. The method by which the neutron scattering and capture gamma values were obtained has already been described. The curve labeled "reactor gammas" is based on a geometry like that in the present calculation (reactor point source model, 10 ft separation, and identical tank end configuration) for which computer integrations[4] were performed on the direct, first scattered, and buildup heating contributions delivered by eight monoergic gamma ray sources whose intensity was adjusted to represent the effective axial leakage from a reactor as seen from the tank location.*

Considering the effect of all the nuclear radiation

---

*These reactor gamma calculations will be covered in detail in another report.

sources, Figure 28, one notes that the present Monte Carlo study on neutron heating extended to an adequate propellant depth, since ~98 percent of the heating comes from nonneutron sources at the 92 cm plane at which the present problem was terminated.

In spite of the fact that reactor neutrons directly carry only about 25 percent of the total energy imparted to the propellant by reactor leakage radiation, theirs is the major contribution near the front face of the tank where the heating is raised to several times that from reactor gammas alone. Without heat transfer, the maximum power input shown would produce a temperature rise rate of approximately 0.3°C/sec (based on a specific heat for LH_2 of 2.25 cal/gm-°C). Of course, the practical effect of such heating rates on questions of pump cavitation, tank pressure rise, and propellant boiloff would depend on the time for which this rise rate was sustained, the degree of mixing, and the rate of propellant removal. Such a high-valued, high-gradient heating source could be coped with readily under many conditions of "potential flow," even without a shield,[4] but the greater likelihood of a nearly uncontrolled propellant circulation may force the inclusion of a shield to preclude the possibility of intolerable temperature rises in the propellant.

APPENDIX

The group cross sections and mean free paths for hydrogen scattering as used in this calculation are tabulated below. The LH_2 (liquid hydrogen) density used was 0.07 gm/cm^3. The upper bound of the first energy group is 8 Mev.

Lower Bound of Group Energy (Mev)	σ (barns)	Σ (cm^{-1})	λ (cm)
7.25	1.18	0.04937	20.26
6.50	1.27	0.05314	18.82
6.00	1.38	0.05774	17.32
5.50	1.47	0.06150	16.26
5.00	1.56	0.06527	15.32
4.50	1.70	0.07113	14.06
4.00	1.82	0.07615	13.13
3.75	1.93	0.08075	12.38
3.50	2.01	0.08410	11.89
3.25	2.11	0.08828	11.33
3.00	2.20	0.09205	10.86
2.80	2.32	0.09707	10.30
2.60	2.42	0.1013	9.872
2.40	2.55	0.1067	9.372
2.20	2.67	0.1117	8.953
2.00	2.81	0.1176	8.503
1.80	2.98	0.1247	8.019
1.60	3.17	0.1326	7.541
1.40	3.40	0.1423	7.027
1.30	3.60	0.1506	6.640
1.20	3.75	0.1569	6.373
1.10	3.93	0.1644	6.083
1.00	4.13	0.1728	5.787
0.90	4.38	0.1833	5.456

Lower Bound of Group Energy (Mev)	σ (barns)	Σ (cm^{-1})	λ (cm)
0.80	4.65	0.1946	5.139
0.70	4.98	0.2084	4.798
0.60	5.38	0.2251	4.442
0.50	5.85	0.2448	4.085
0.45	6.30	0.2636	3.794
0.40	6.68	0.2795	3.578
0.35	7.15	0.2992	3.342
0.30	7.60	0.3180	3.145
0.25	8.25	0.3452	2.897
0.20	9.05	0.3787	2.641
0.15	10.10	0.4226	2.366
0.125	11.20	0.4686	2.134
0.10	12.05	0.5042	1.983
0.09	12.8	0.5356	1.867
0.08	13.3	0.5565	1.797
0.06	14.1	0.5899	1.695
0.04	15.4	0.6443	1.552
0.03	16.5	0.6904	1.448
0.017	17.5	0.7322	1.366
0.010	18.5	0.7740	1.292

The elastic scattering equations take on a rather simple form for collisions with hydrogen. If θ is the scattering angle in the center-of-mass system and ψ is the scattering angle in the laboratory system, then

$$\psi = \frac{\theta}{2}$$

This relation shows that the neutron can never scatter more than 90° in the laboratory system - i.e., there is no back-scatter from a single collision. The energy E' of a scattered neutron is related to its original energy E_o by the

expression:

$$E' = E_o \frac{(1 + \cos \theta)}{2} = E_o \cos^2 \frac{\theta}{2}$$

Since isotropic scattering distributes the scattered vectors uniformly over cos θ ($-1 \leq \cos \theta \leq +1$), all energies E' between zero energy and E_o are equally probable. The average energy loss per collision (or the residual energy after collision) is $E_o/2$, and the average energy of all neutrons scattered below an energy E_C is $E_C/2$. Thus the average energy carried by the neutrons whose histories were cut off in this Monte Carlo calculation upon scatter below 10 kv should be 5 kv, and, as a check, this result was obtained to a very high order of accuracy whenever a large number of cutoffs were described.

The neutron energy loss was always assumed to be deposited at the point of collision, since recoil protons (hydrogen atoms) possessing as much as 4 Mev of energy would travel only 1 to 1.5 mm in LH_2.

Scattering histories were developed through random number generation in the IBM 704 computer, with each such number resulting in an assignment of one or more of the particle or history parameters via their correspondence to values along the range of precalculated probability integrals - e.g., the random number r ($0 \leq r \leq 1$) could assign the

post-collision energy E' by the relationship $E' = rE_o$ and the laboratory scattering angle ψ through the relationship $\cos \psi = \sqrt{r}$.

Discussions of the Monte Carlo methods involved in such procedures may be found in several places, among which the book[5] by Cashwell and Everett may prove to be of particular value to the reader.

REFERENCES

(1) D. J. Hughes and R. B. Schwartz, "Neutron Cross Sections, Second Edition," Brookhaven National Laboratory Report BNL-325, July, 1958.

(2) M. O. Burrell, "Nuclear Radiation Transfer and Heat Deposition Rates in Liquid Hydrogen," NASA Technical Note, D-1115, August, 1962.

(3) W. L. Whittemore and A. W. McReynolds, "Differential Neutron Thermalization," General Atomics Report GA-2503, September 30, 1961.

(4) G. A. Graves and J. R. Streetman, "Radiation Heating in the Liquid Hydrogen Propellant of Nuclear Rockets," Trans. Am. Nucl. Soc., Vol. 4, No. 1, 165, June, 1961.

(5) E. D. Cashwell and C. J. Everett, "A Practical Manual on the Monte Carlo Method for Random Walk Problems," Pergamon Press, 1959.

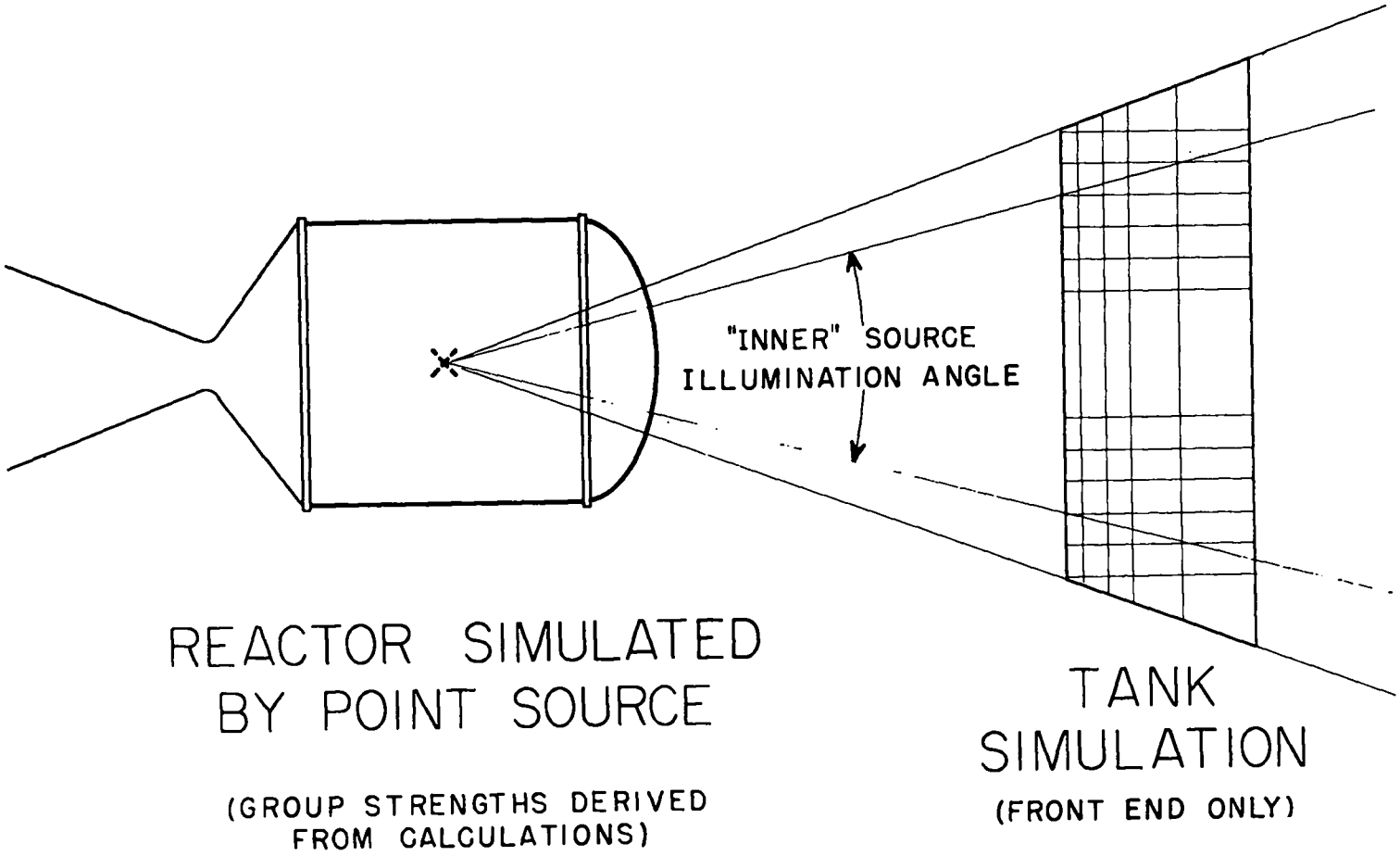

Fig. 1. Overall geometry simulated by problem

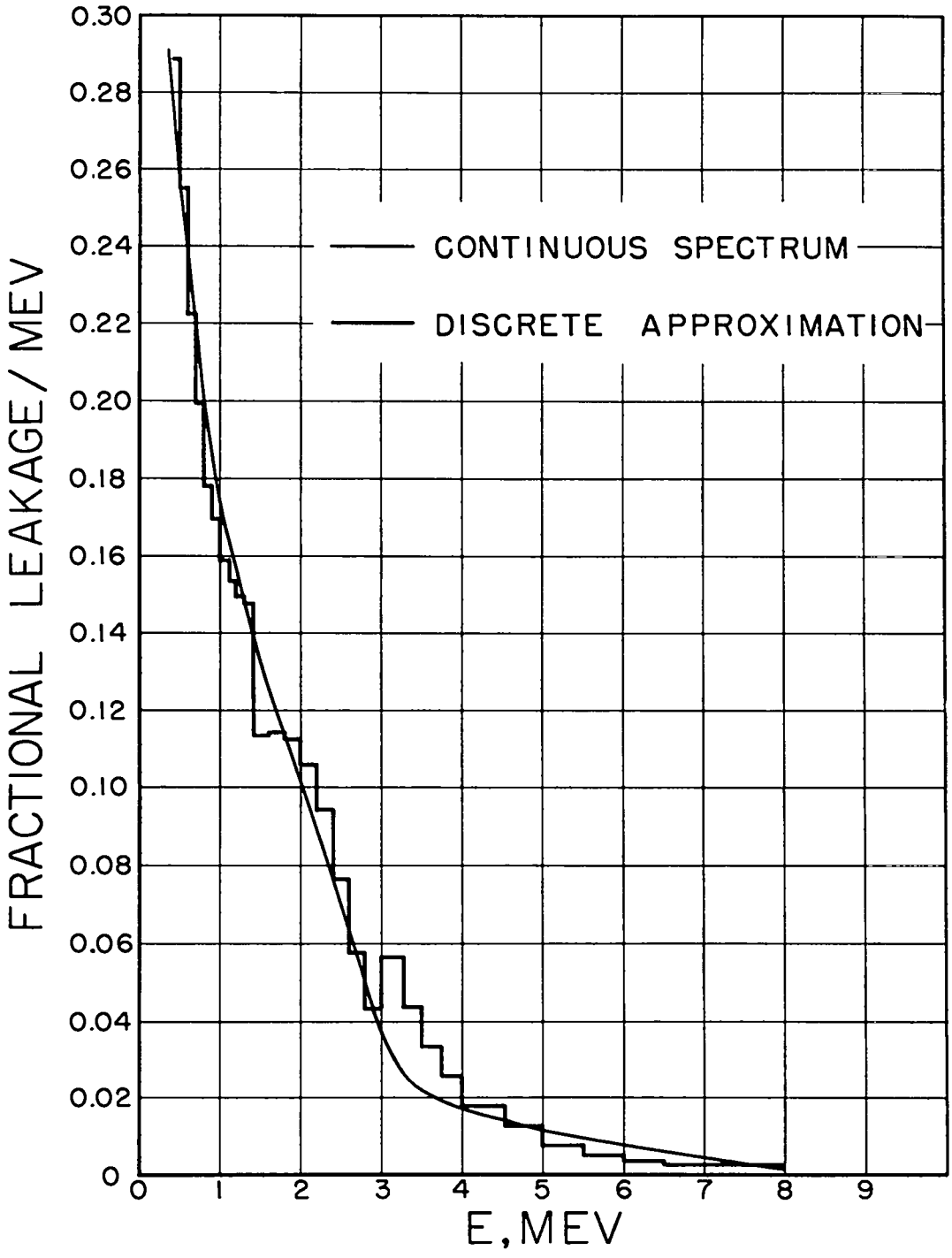

Fig. 2. Neutron spectrum approximated

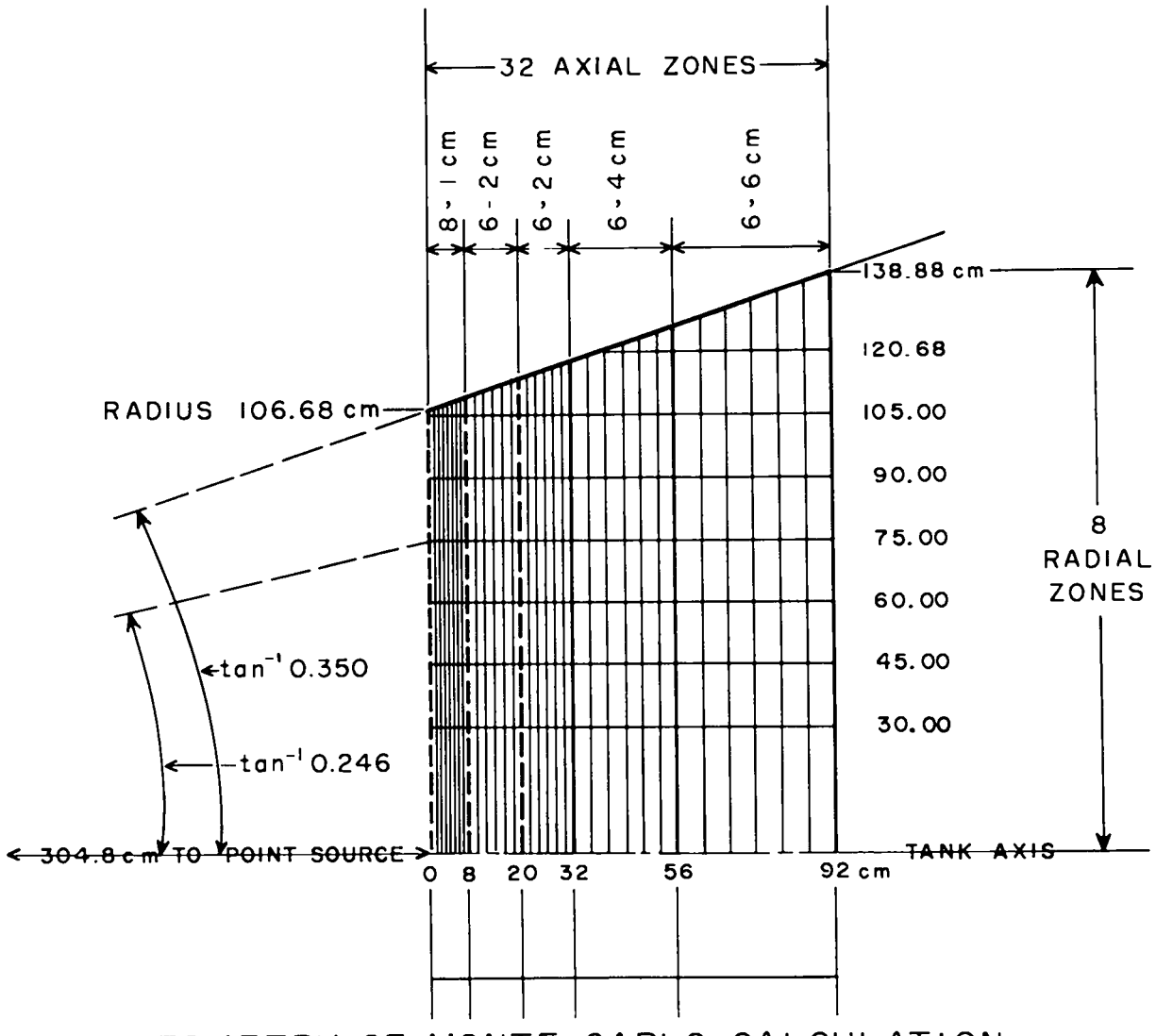

Fig. 3. Detailed tank geometry

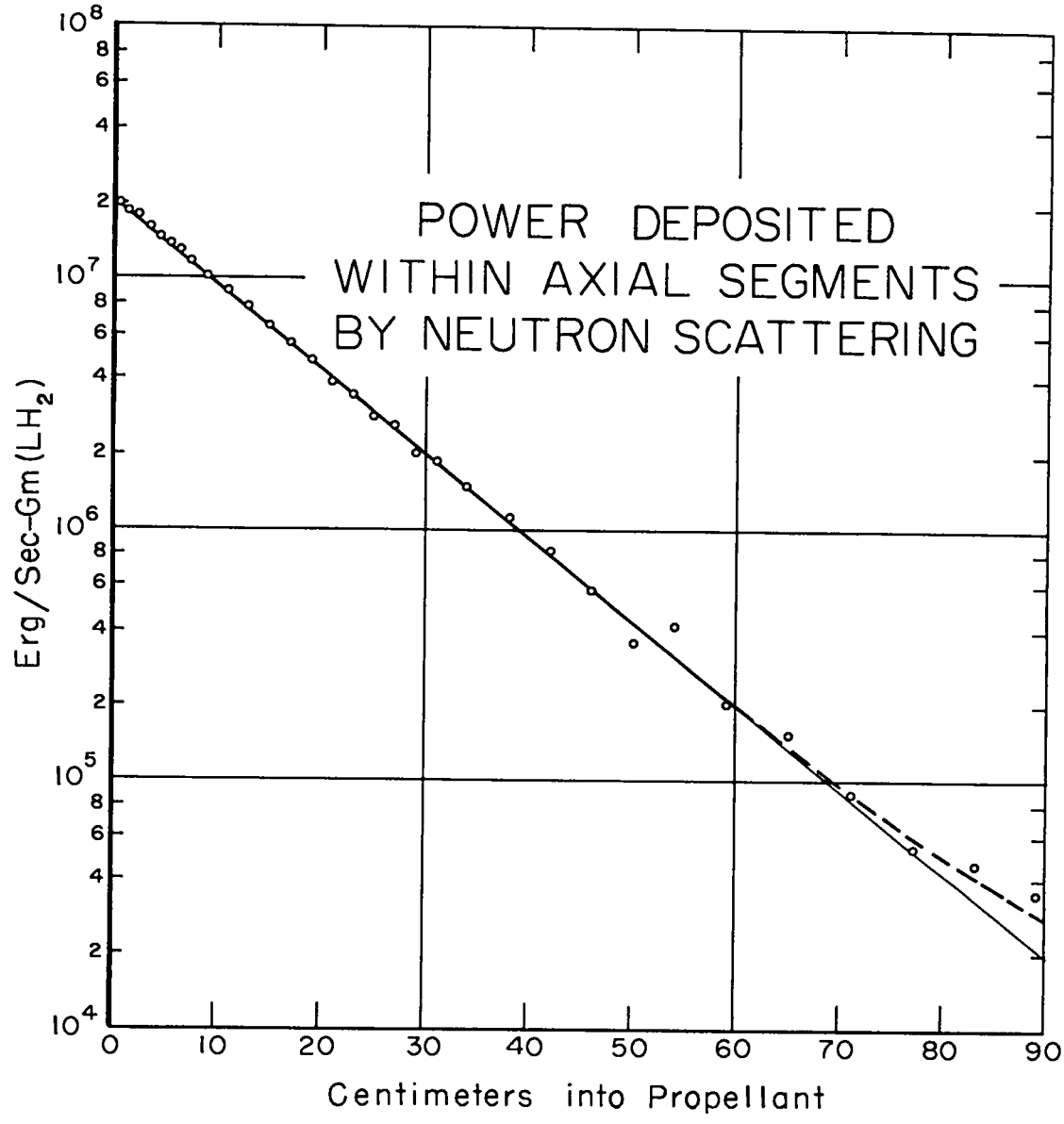

Fig. 4. Total power generation near axis by neutrons

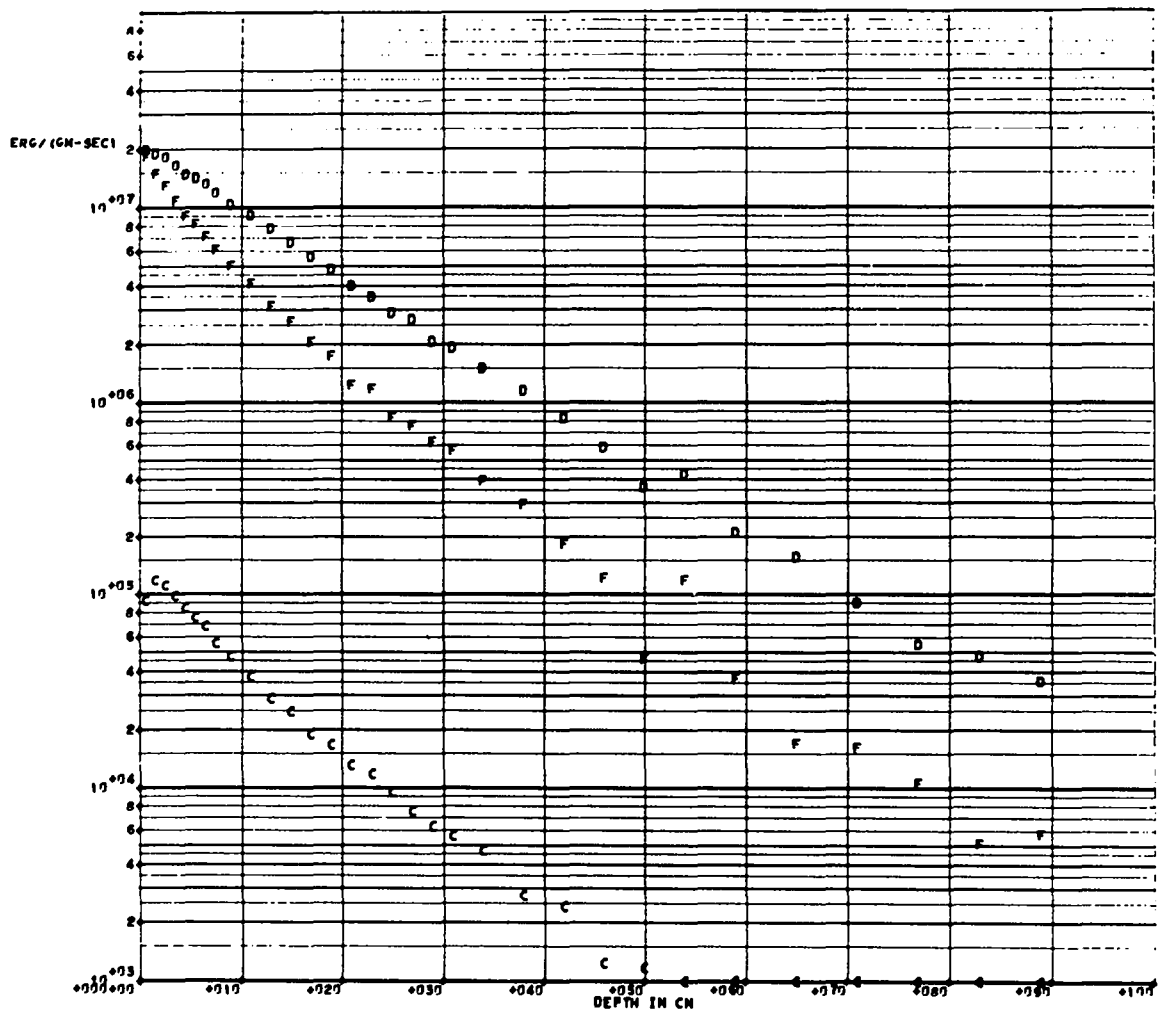

Fig. 5. First collision (F), cutoff (C), and total energy deposition (D) rates versus depth for the inner segment

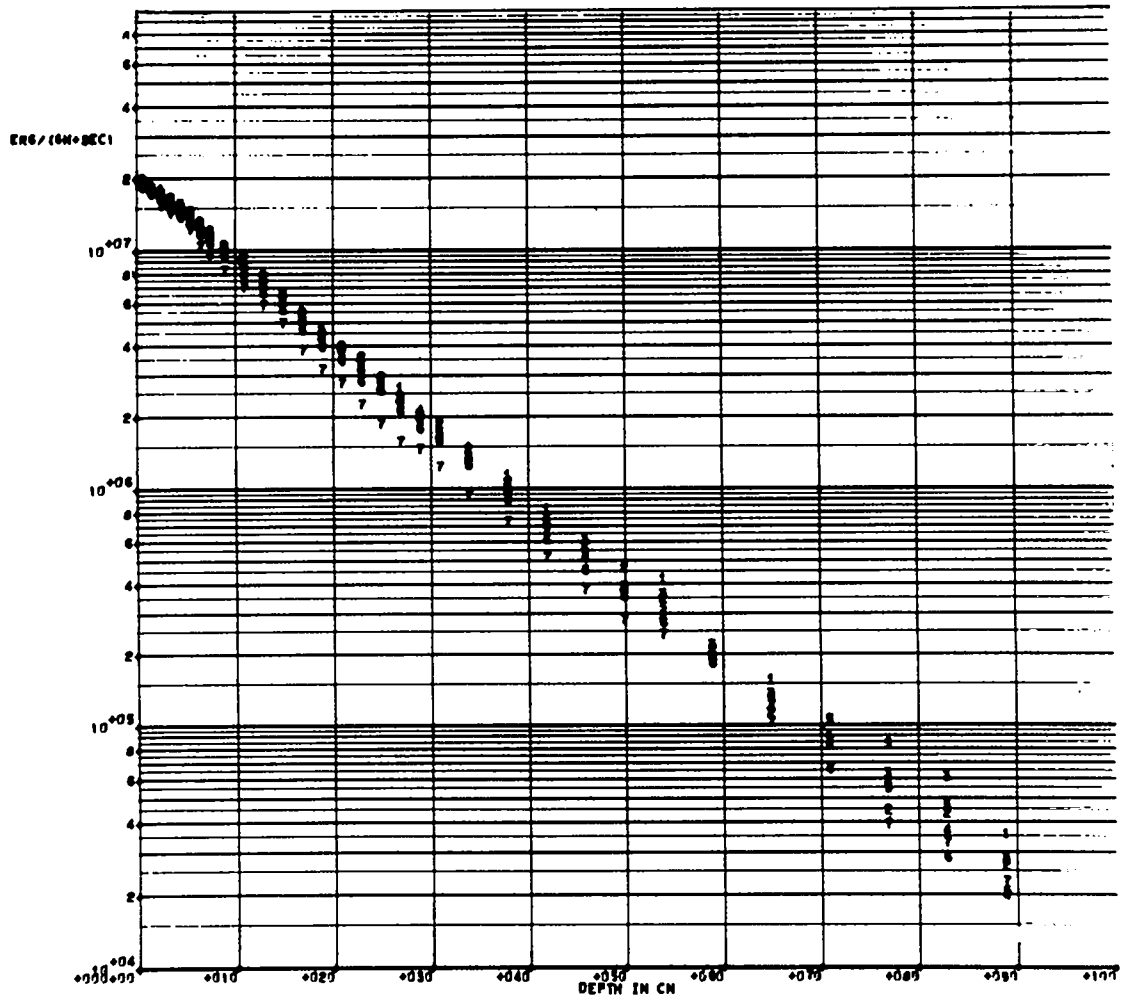

Fig. 6. Total power generation by depth and radial segment number

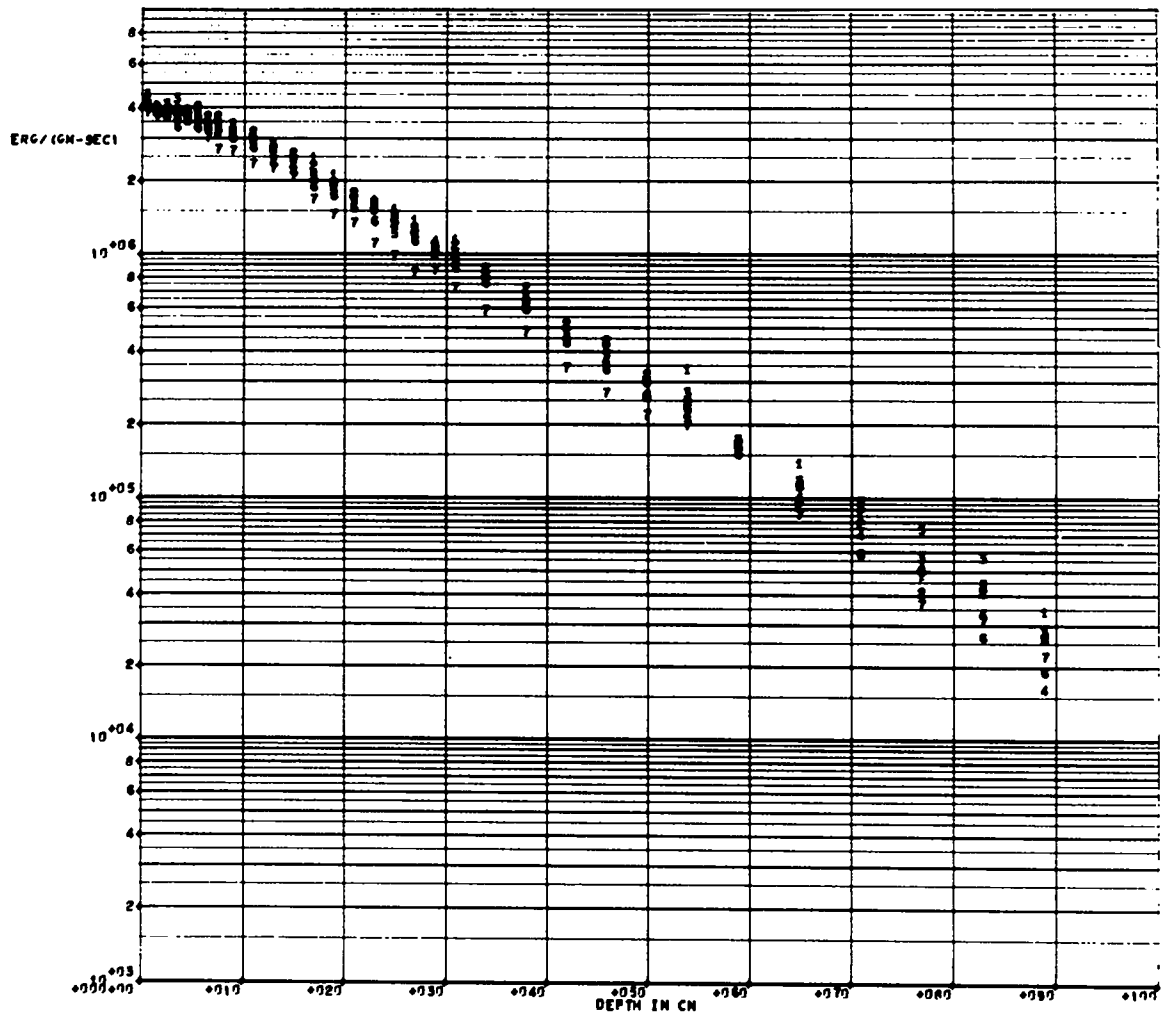

Fig. 7. Power generation from group 1 by depth and radius

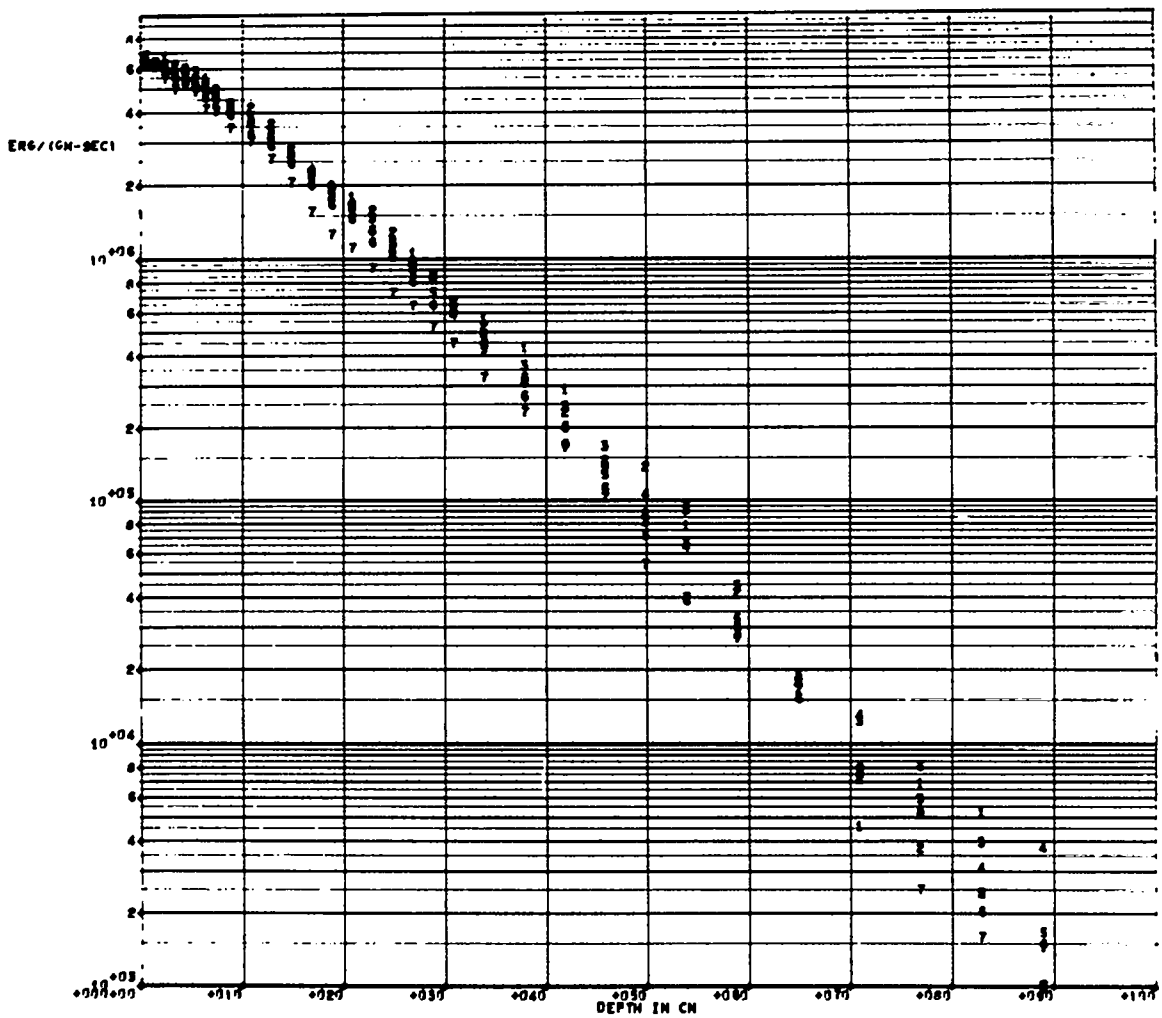

Fig. 8. Power generation from group 2 by depth and radius

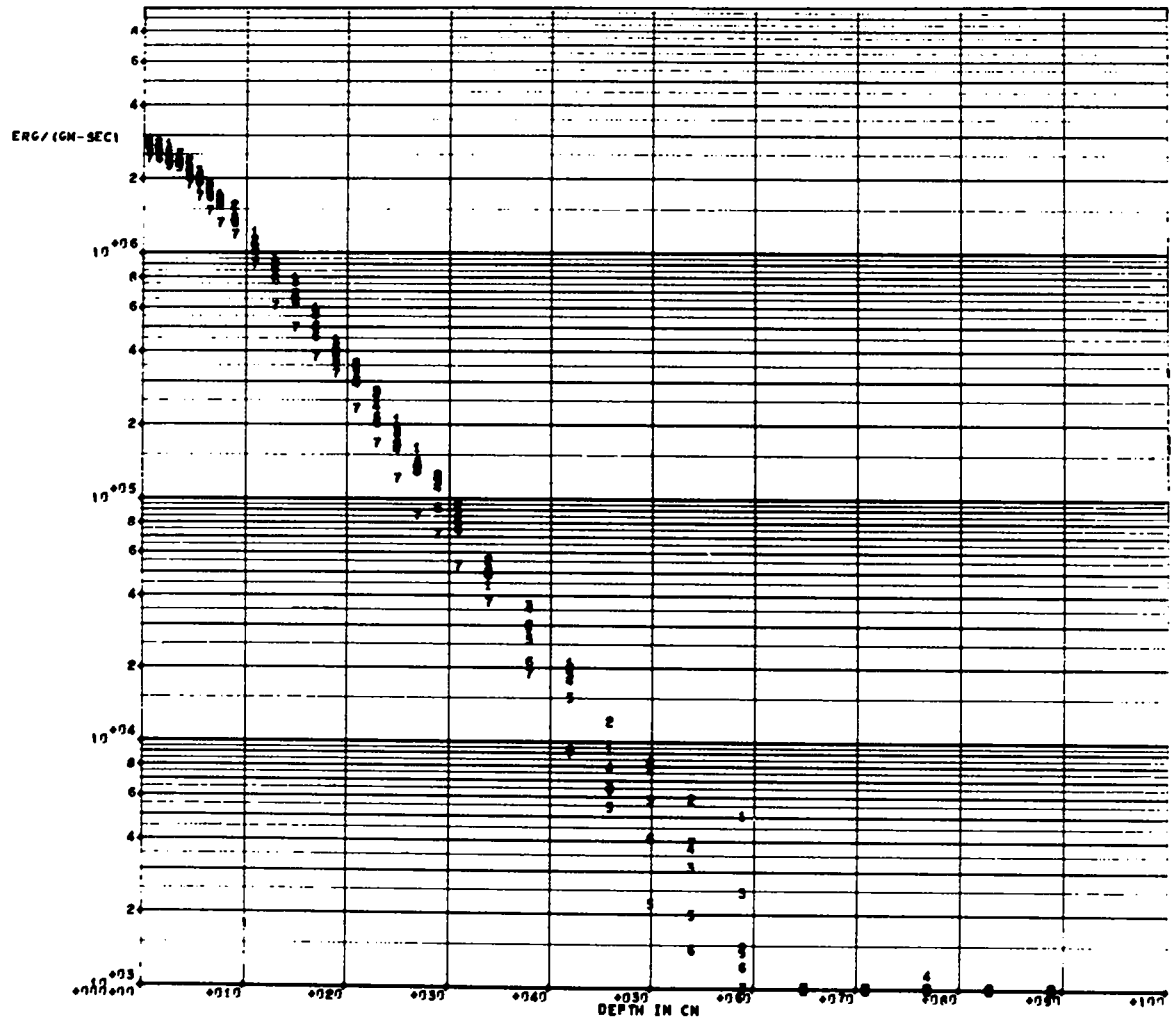

Fig. 9. Power generation from group 3 by depth and radius

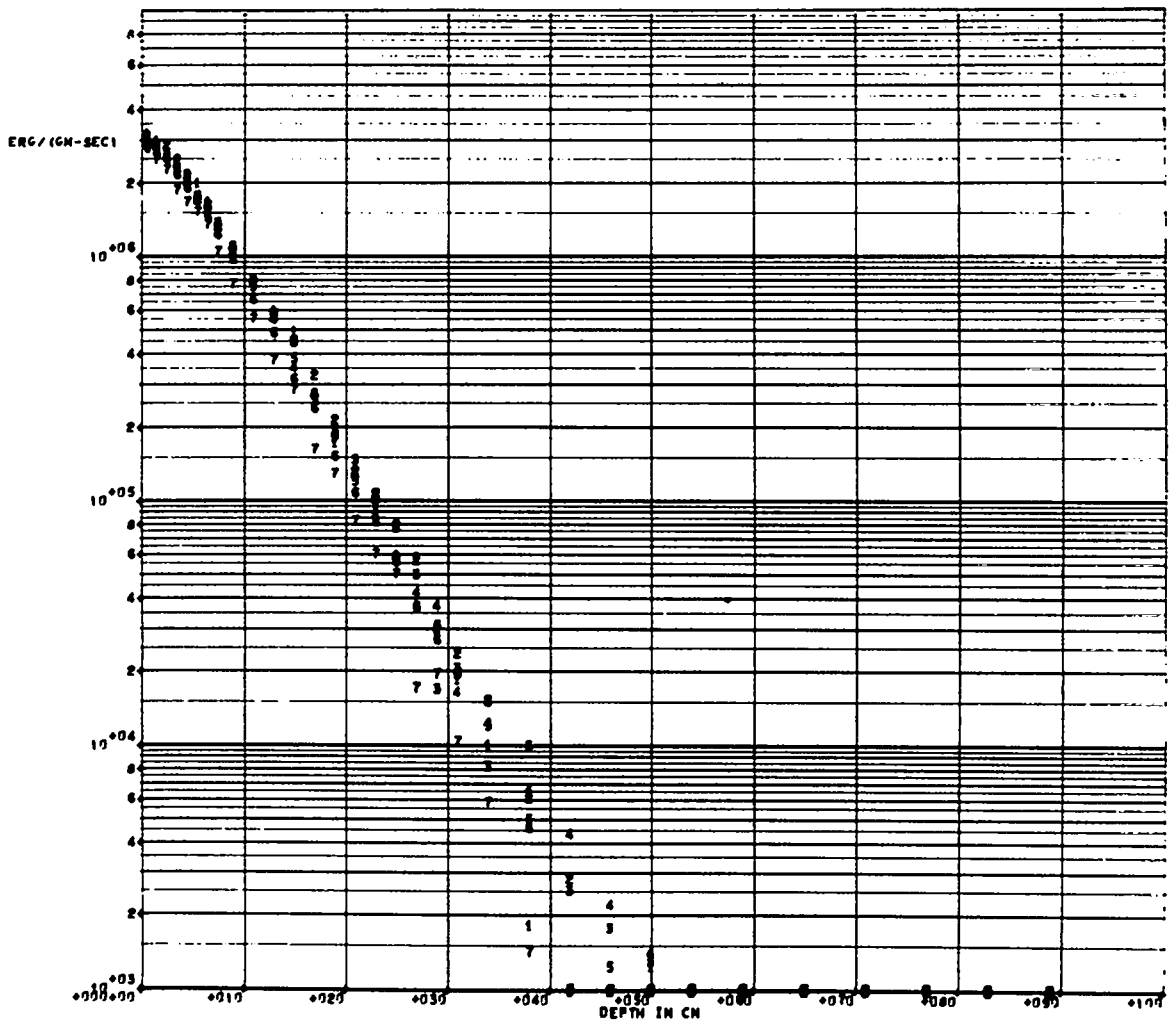

Fig. 10. Power generation from group 4 by depth and radius

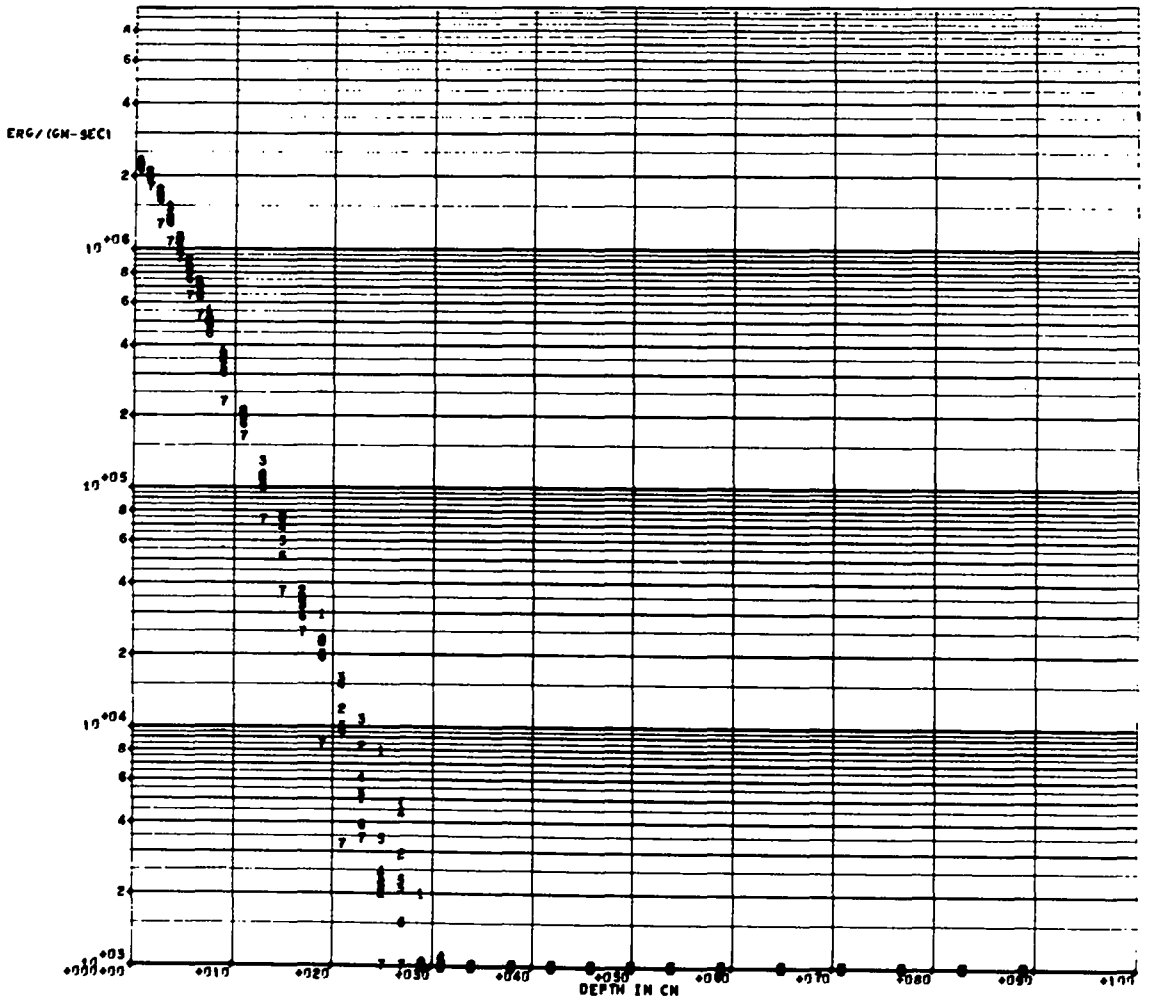

Fig. 11. Power generation from group 5 by depth and radius

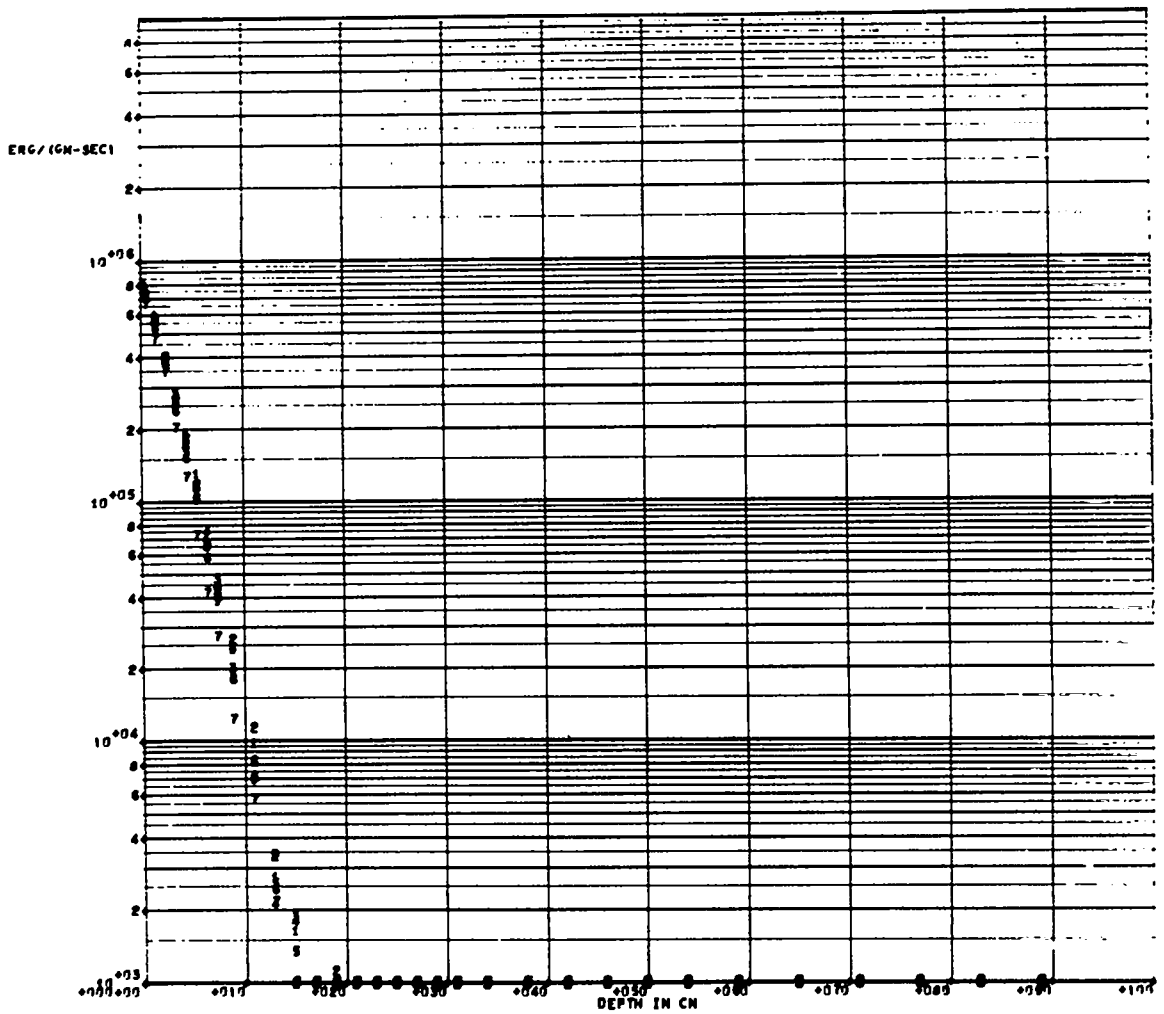

Fig. 12. Power generation from group 6 by depth and radius

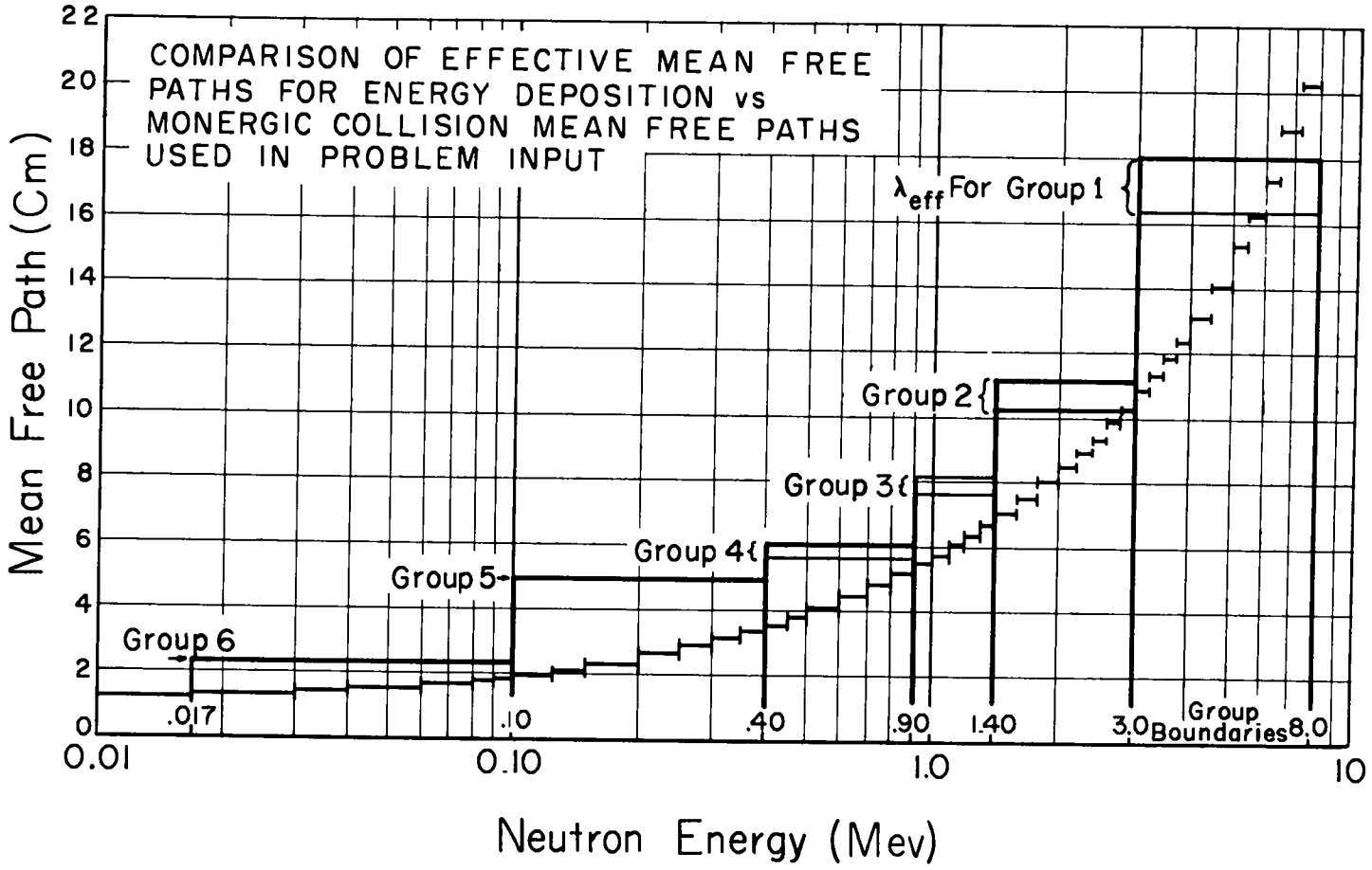

Fig. 13. "Effective" versus monoergic mean free paths

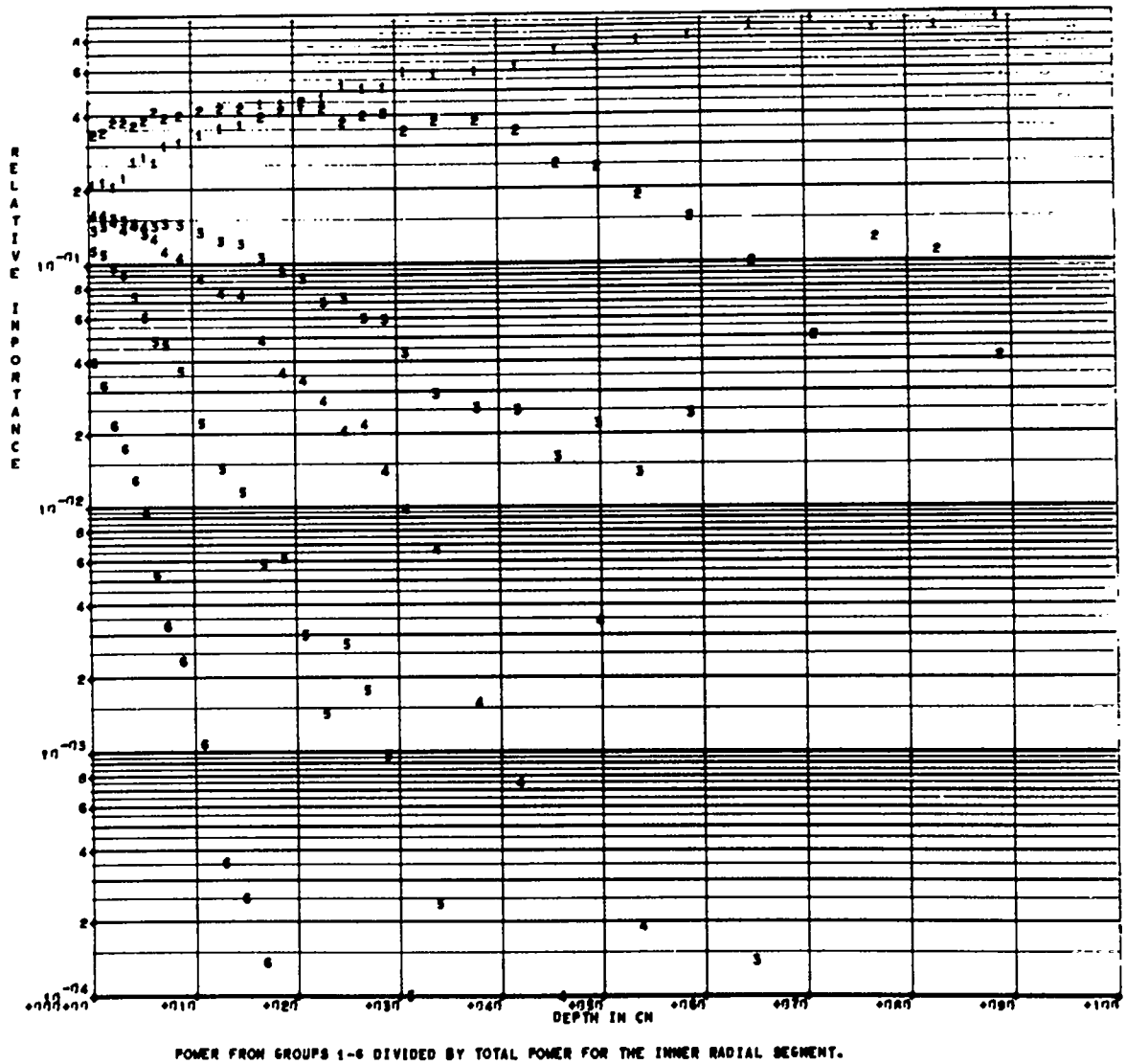

Fig. 14. Relative group importance to energy deposition versus depth

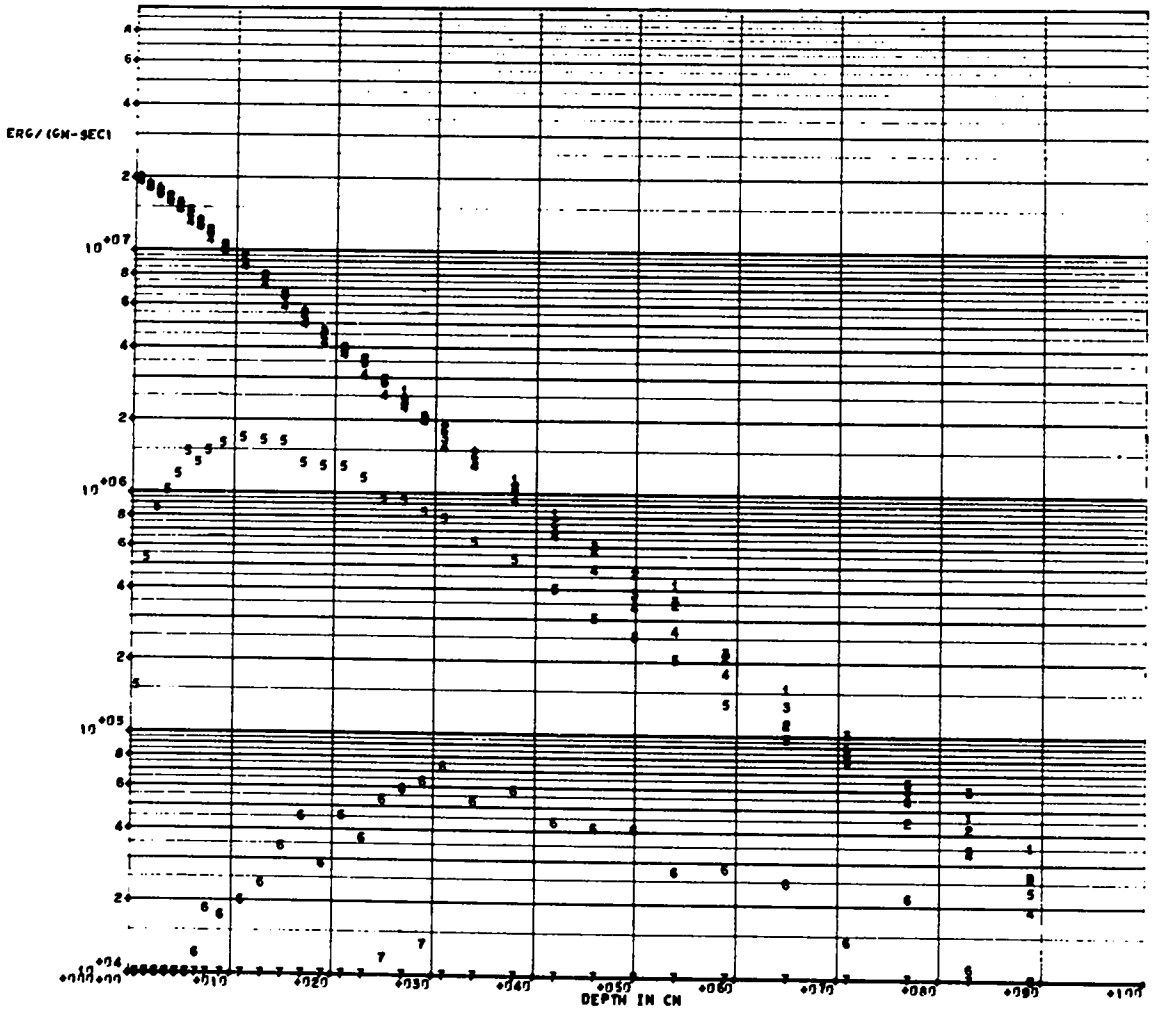

Fig. 15. Inner neutrons: total power generation by depth and radial segment number

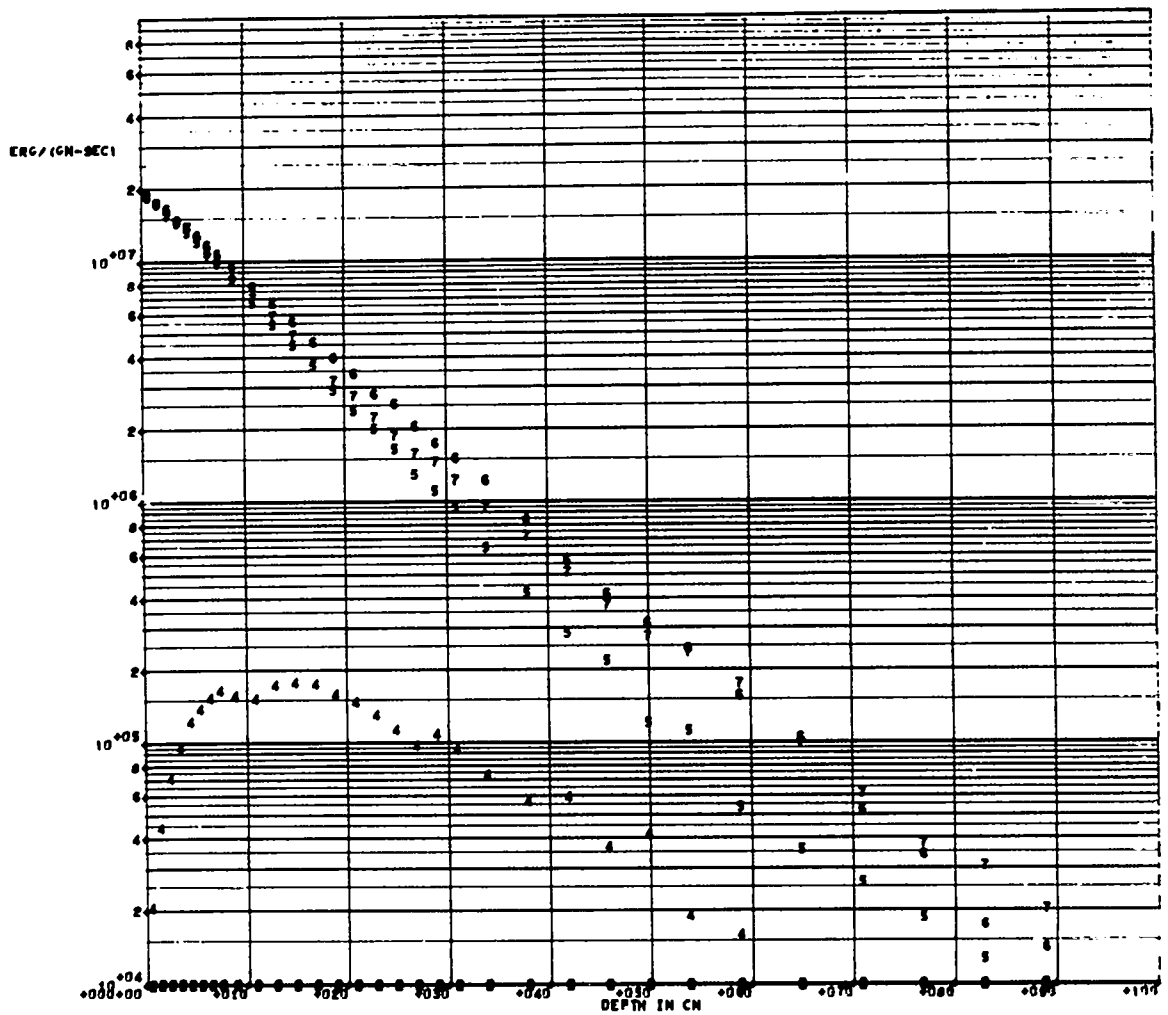

Fig. 16. Outer neutrons: total power generation by depth and radial segment number

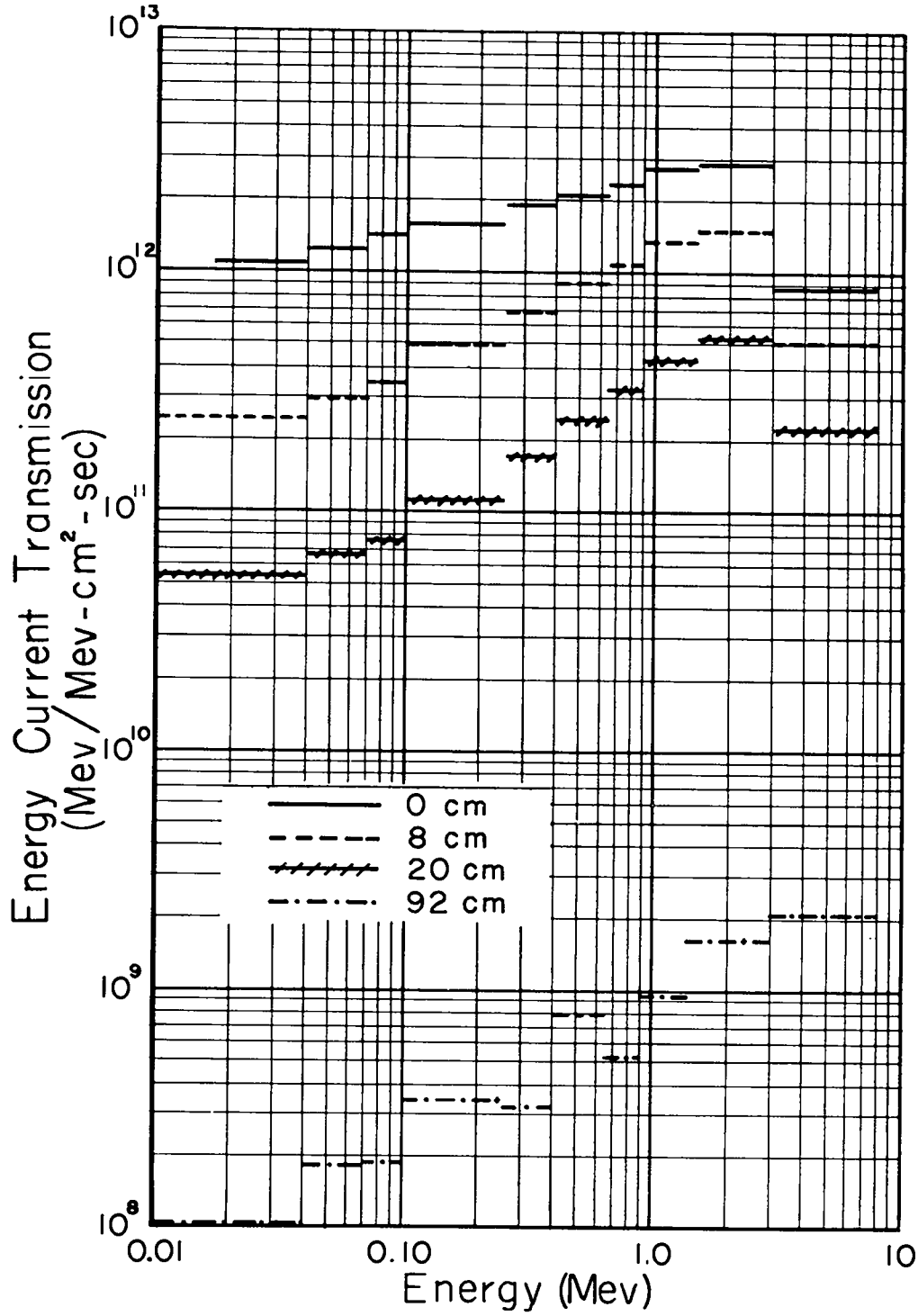

Fig. 17. Spectra transmitted through planes at 0, 8, 20, and 92 cm depth

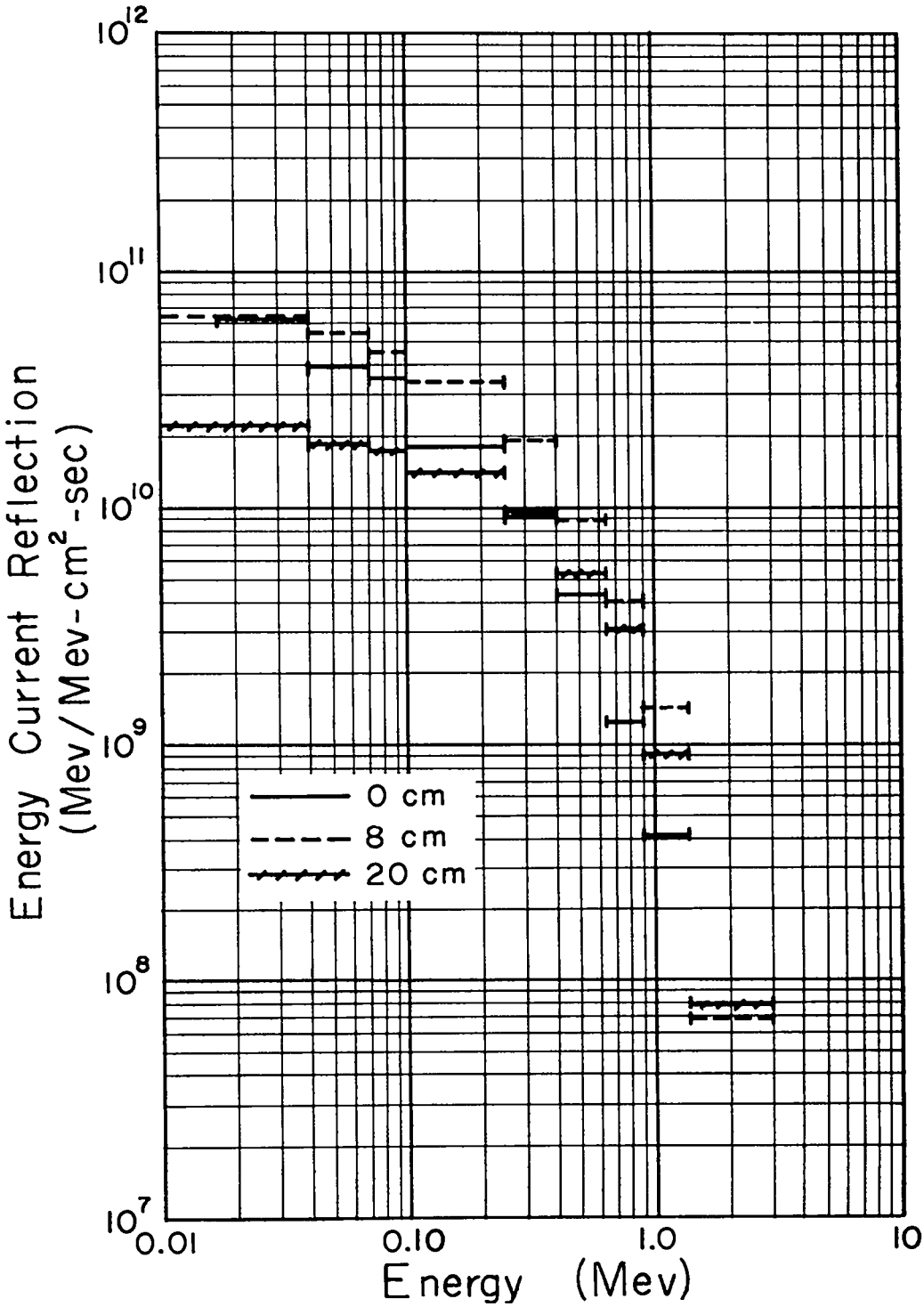

Fig. 18. Spectra reflected by planes at 0, 8, and 20 cm depth

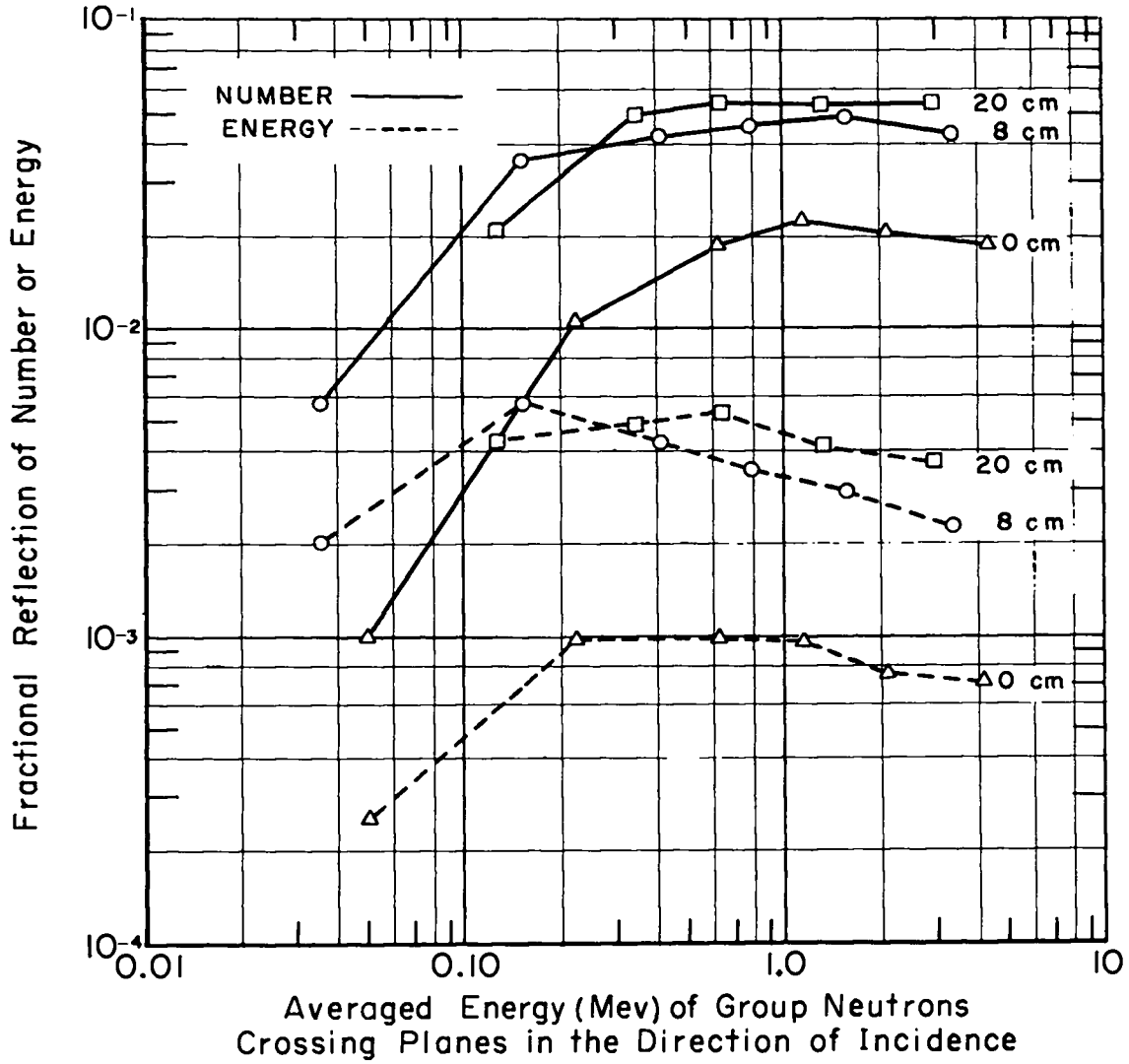

Fig. 19. Fractional reflection of neutrons and neutron energy versus average energy at incidence on planes at 0, 8, and 20 cm depth

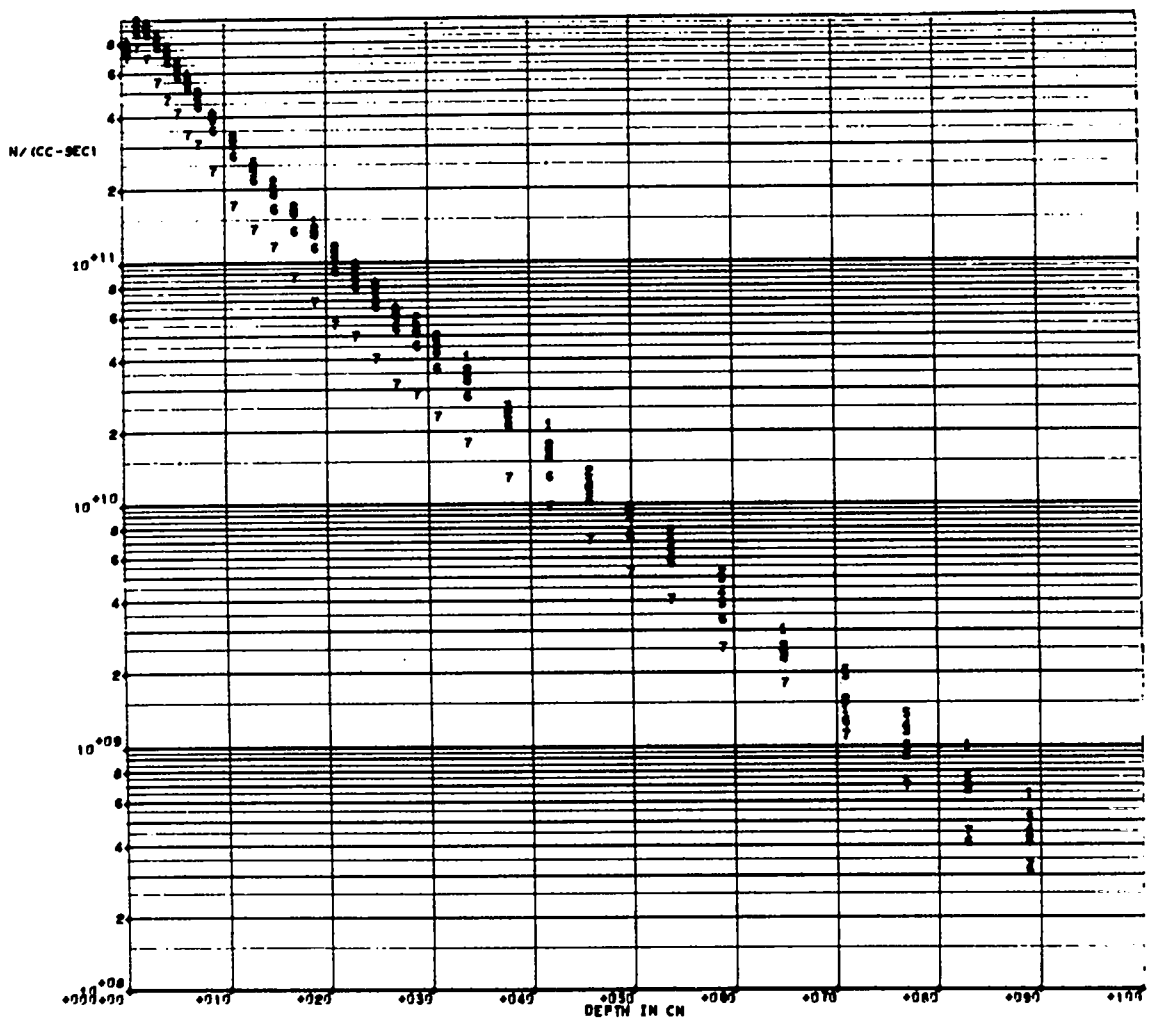

Fig. 20. Total neutron cutoff rate by depth and radial segment number

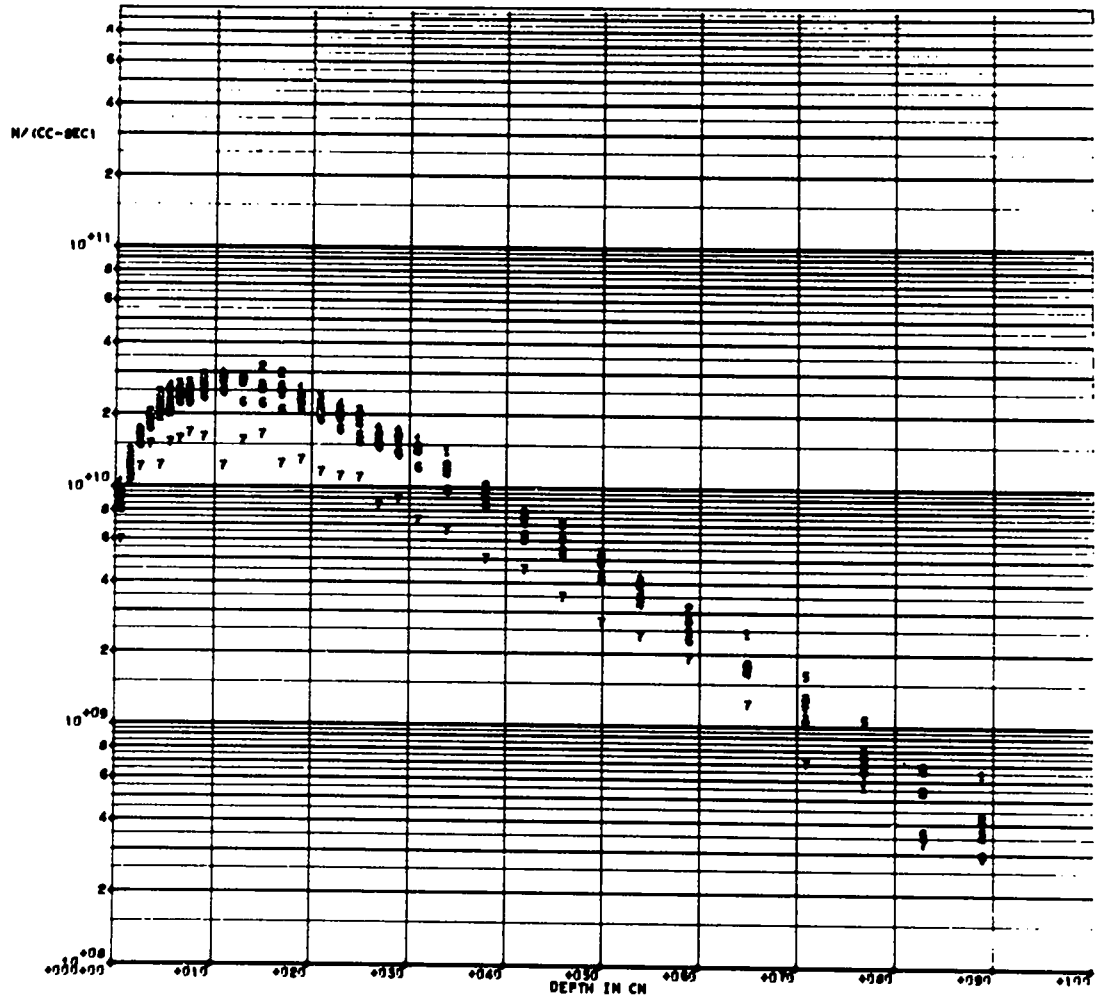

Fig. 21. Neutron cutoff rate in group 1 by depth and radius

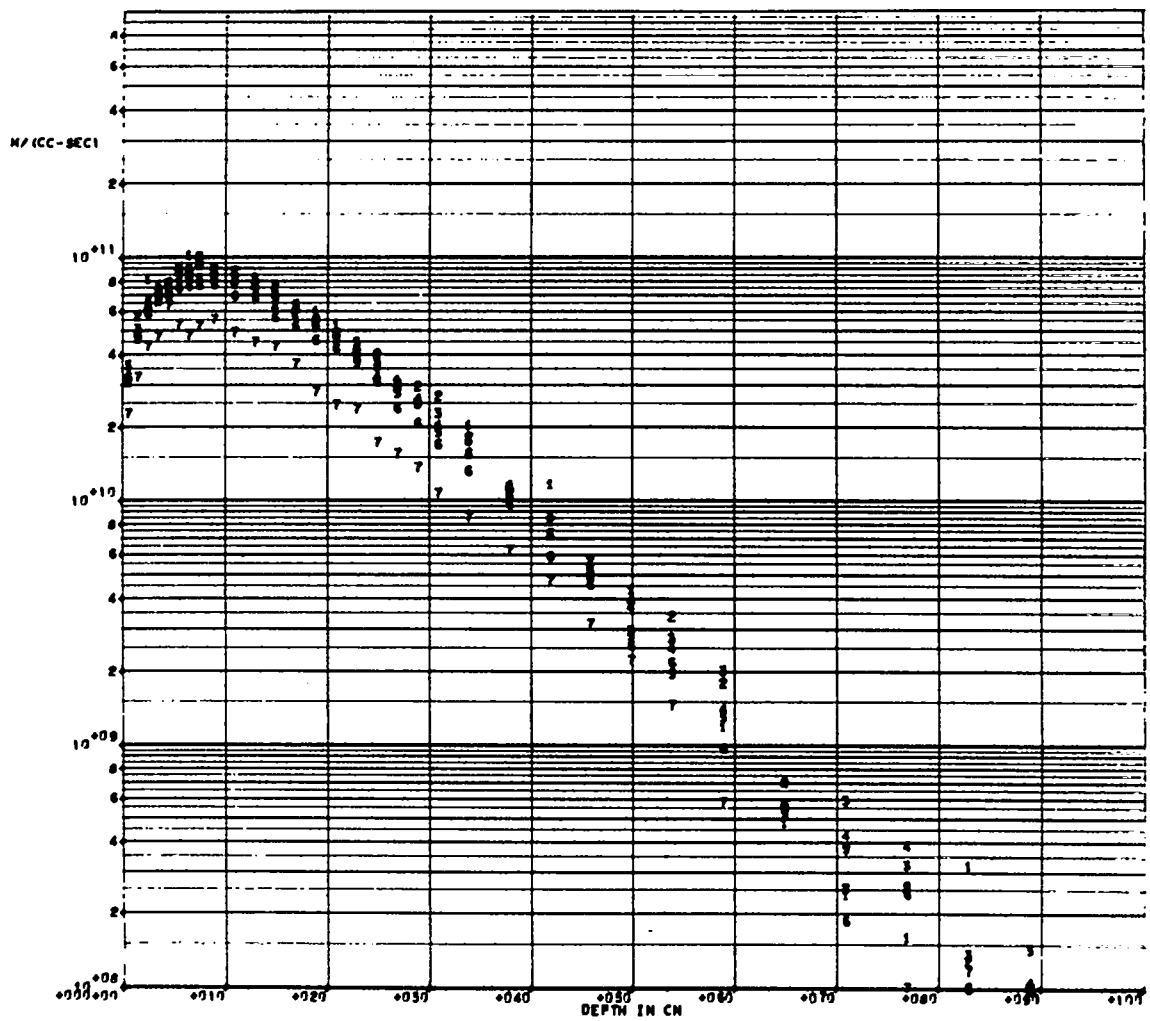

Fig. 22. Neutron cutoff rate in group 2 by depth and radius

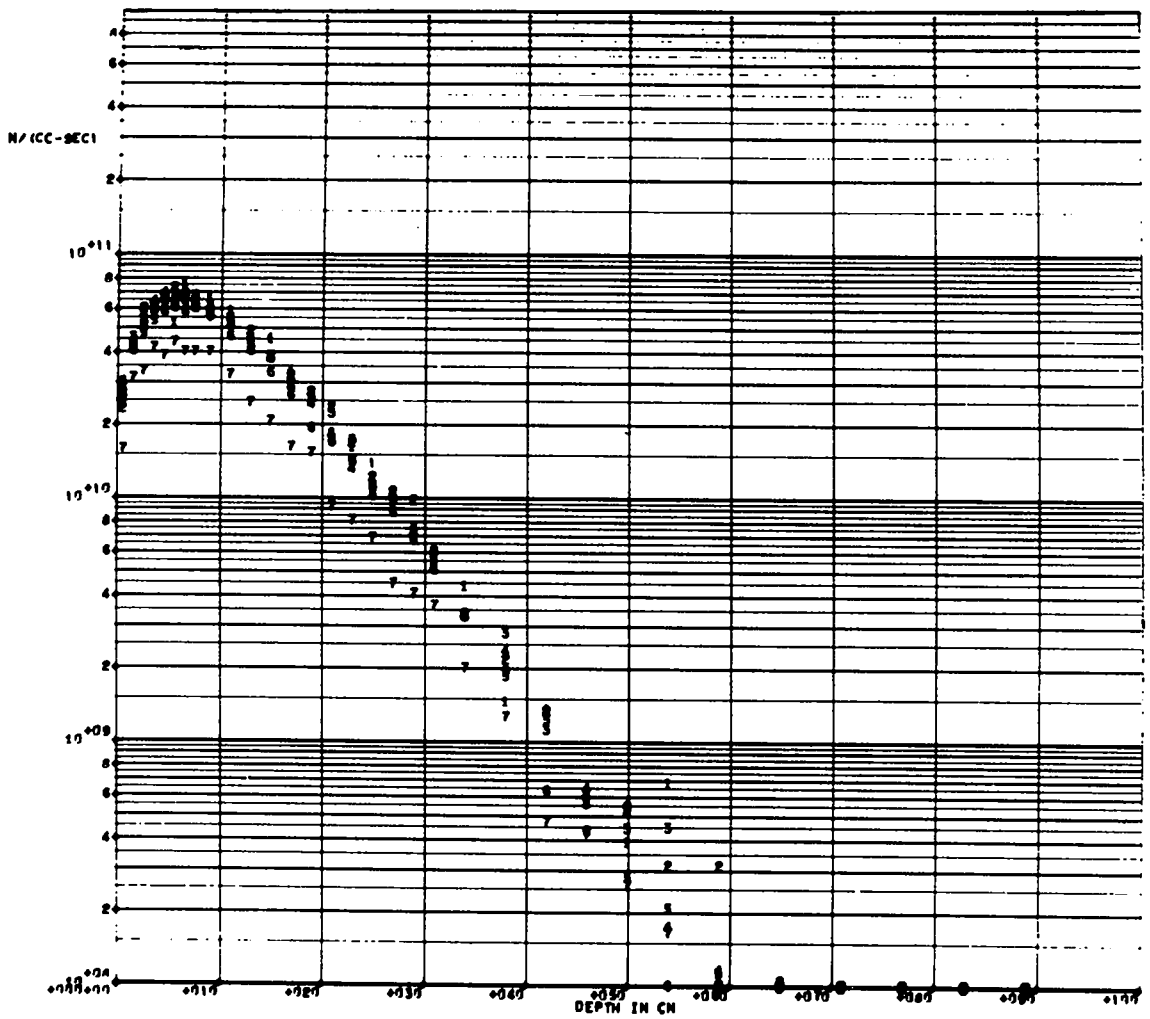

Fig. 23. Neutron cutoff rate in group 3 by depth and radius

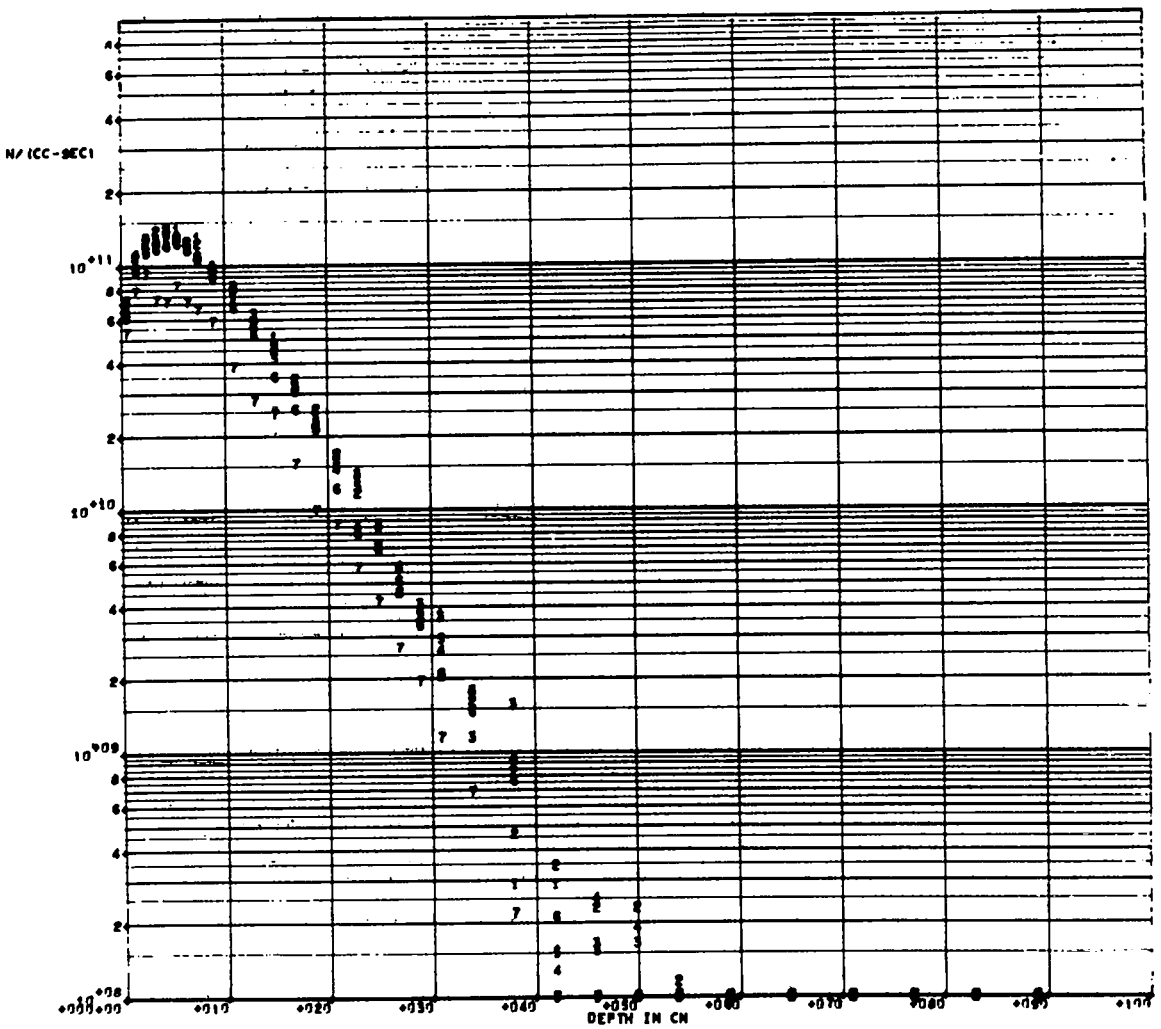

Fig. 24. Neutron cutoff rate in group 4 by depth and radius

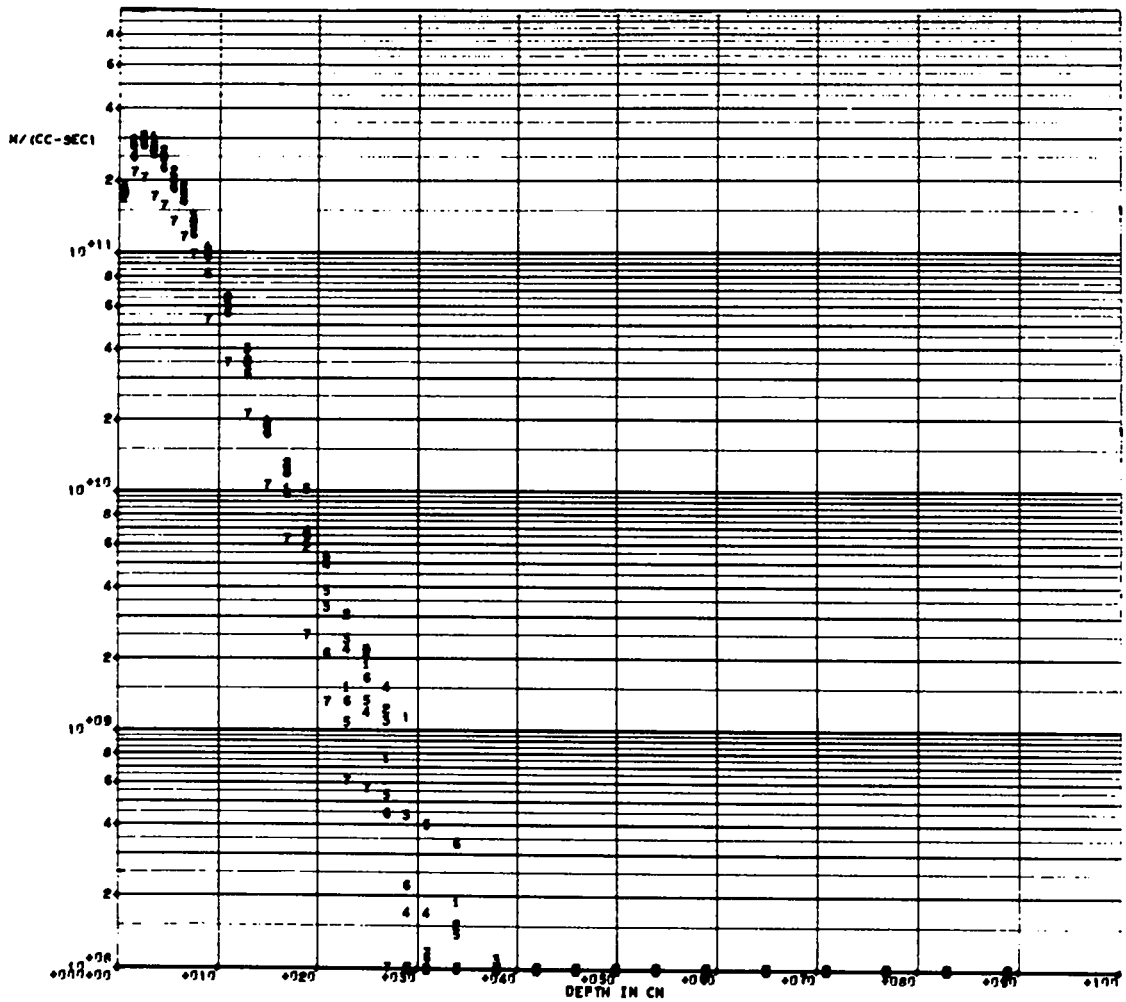

Fig. 25. Neutron cutoff rate in group 5 by depth and radius

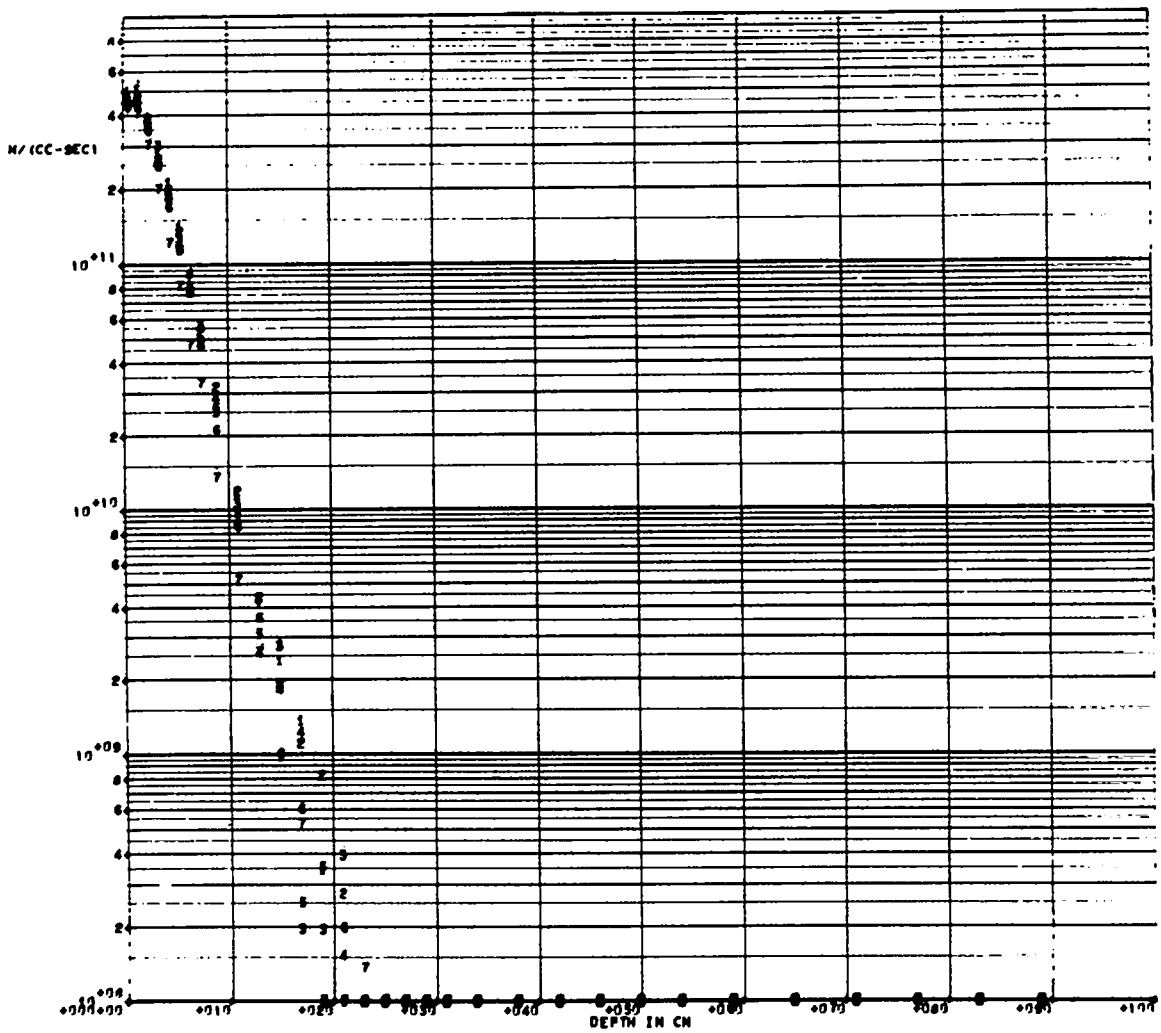

Fig. 26. Neutron cutoff rate in group 6 by depth and radius

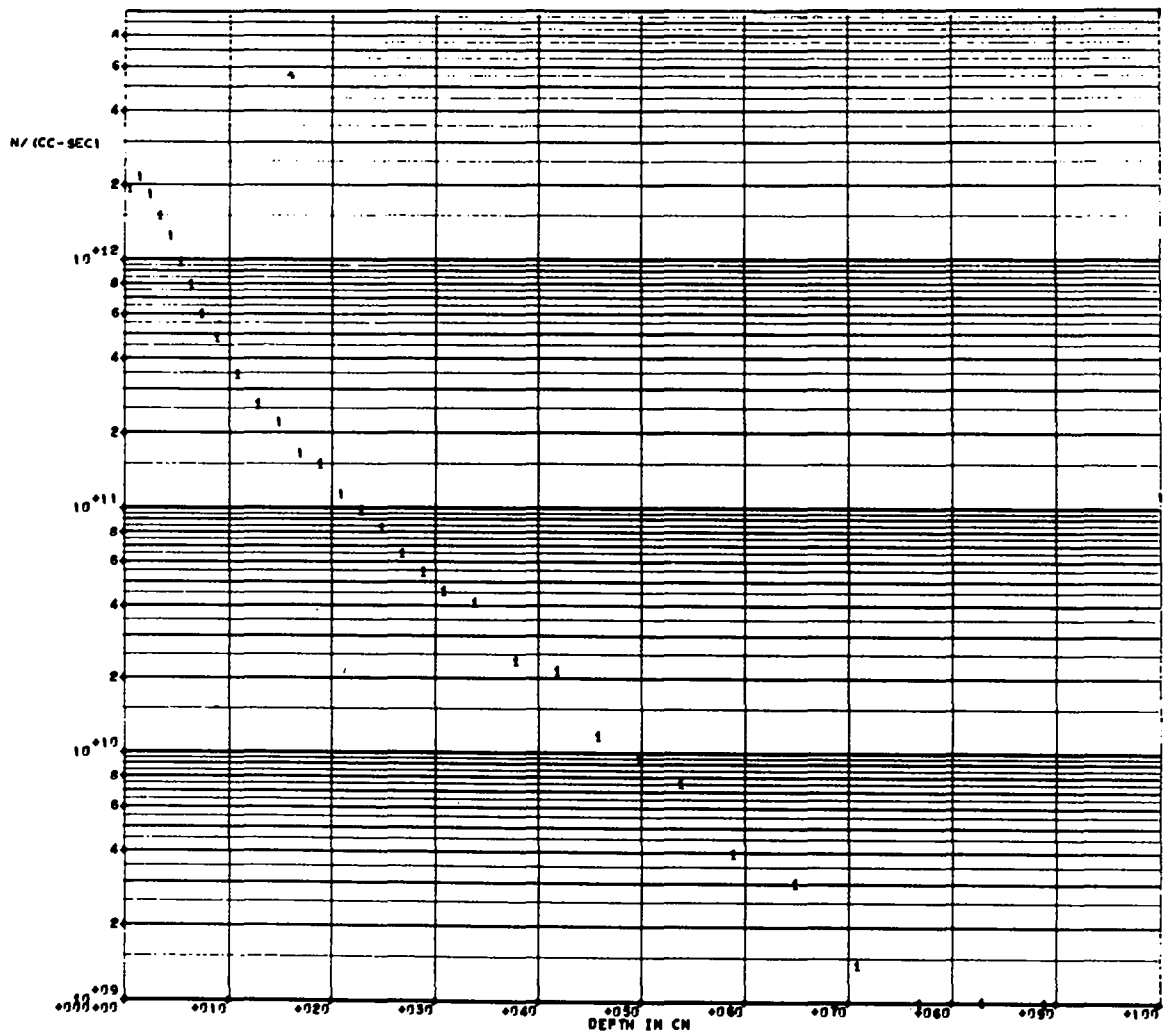

Fig. 27. Postulated axial capture distribution (total neutron cutoff rate in first radial segment with group 6 values increased for low energy neutron contributions)

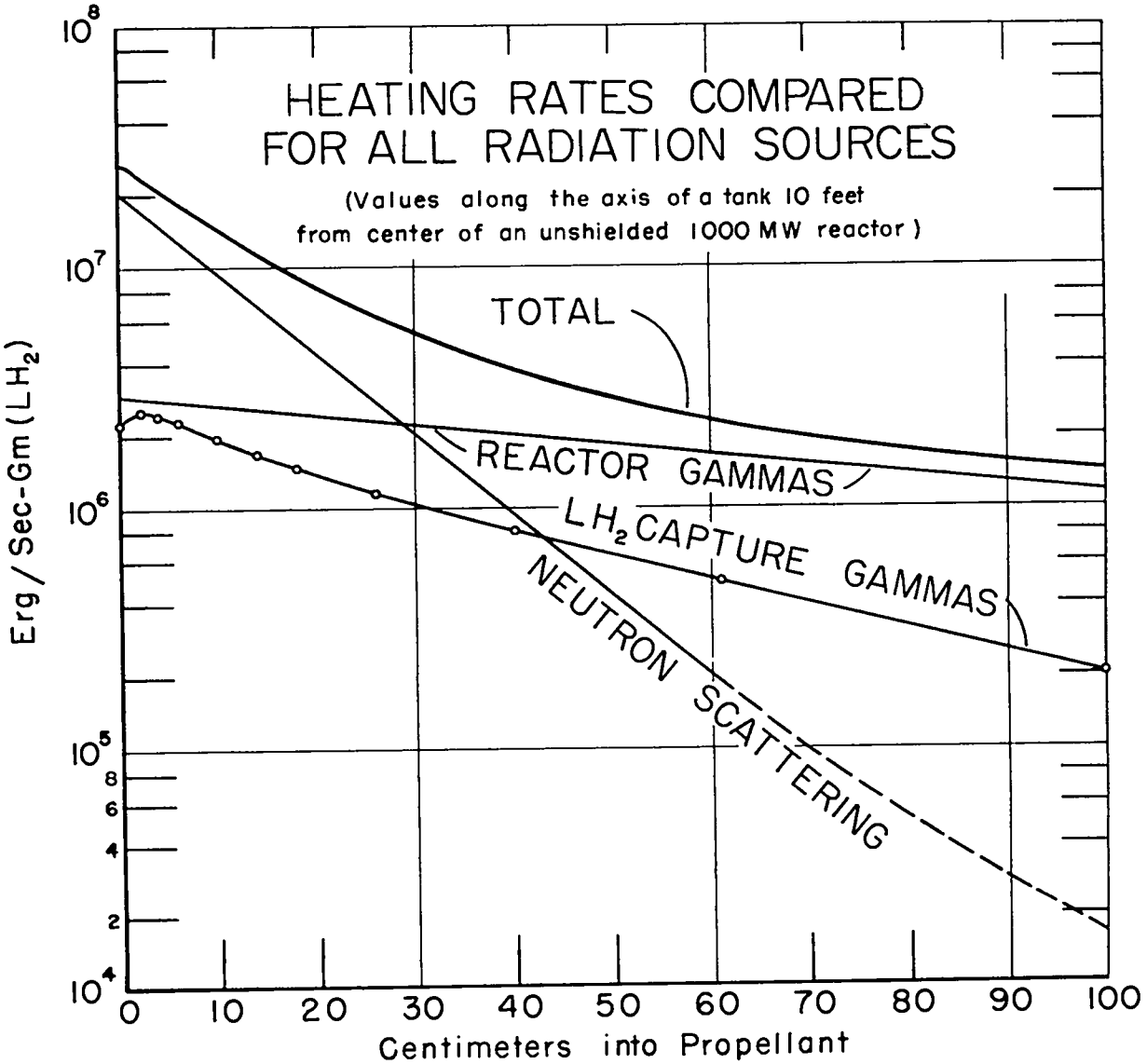

Fig. 28. Heating rates compared for all radiation sources

TABLE I. PRINCIPAL CHARACTERISTICS OF NEUTRON SOURCE GROUPS USED

Source Group	Energy Range (Mev)	Neutron Emission (n/sec)	Energy Emission* (Mev/sec)	Average Energy* (Mev)
1	8.0 - 3.0	$1.34_0 \times 10^{18}$	5.57×10^{18}	4.15_6
2	3.0 - 1.4	$2.83_9 \times 10^{18}$	5.89×10^{18}	2.07_4
3	1.4 - 0.9	$1.54_4 \times 10^{18}$	1.77×10^{18}	1.14_4
4	0.9 - 0.4	$2.26_3 \times 10^{18}$	1.42×10^{18}	0.62_7
5	0.4 - 0.1	$2.99_6 \times 10^{18}$	$0.67_7 \times 10^{18}$	0.22_6
6	0.1 - 0.017	$2.70_3 \times 10^{18}$	$0.13_5 \times 10^{18}$	0.050
Sum 1-6	8.0 - 0.017	$13.68_5 \times 10^{18}$	$15.46_2 \times 10^{18}$	1.13
Below 6	Below 0.017	$6.11_4 \times 10^{18}$	$\sim 0.02 \times 10^{18}$	~ 0.003
TOTAL	8.0 - thermal	1.98×10^{19}	1.55×10^{19}	~ 0.78

*These characteristics, in monoergic isotropic point sources located as indicated in Figure 1, would provide the same energy impingement rates on the tank as those to which each group of this distributed-energy Monte Carlo was normalized.

TABLE II. RATES OF ENERGY DEPOSITION (Erg/gm-sec) FROM SCATTERS AND CUTOFFS, FROM FIRST SCATTERS ONLY, FROM ALL SCATTERS, AND FROM CUTOFFS ONLY, AND RATES OF NEUTRON CUTOFF (Neutrons/cc-sec), ALL VERSUS DEPTH FOR RADIAL SEGMENTS 1 AND 6

RADIAL SEGMENT 1						RADIAL SEGMENT 6				
SCTR+CUT	1ST. SCTR	ALL SCTR	PWR. CUT	NO. CUT	CM	SCTR+CUT	1ST. SCTR	ALL SCTR	PWR. CUT	NO. CUT
2.0285+07	1.8601+07	2.0191+07	9.3965+04	8.2254+11	0- 1	1.8689+07	1.6983+07	1.8600+07	8.8264+04	7.7093+11
1.8929+07	1.5005+07	1.8811+07	1.1768+05	1.0176+12	1- 2	1.7406+07	1.3751+07	1.7304+07	1.0228+05	8.8157+11
1.8205+07	1.2970+07	1.8094+07	1.1109+05	9.7166+11	2- 3	1.6616+07	1.1743+07	1.6516+07	1.0020+05	8.6817+11
1.6497+07	1.0823+07	1.6399+07	9.8247+04	8.6951+11	3- 4	1.4866+07	9.6998+06	1.4778+07	8.7881+04	7.7406+11
1.4943+07	9.0955+06	1.4858+07	8.5239+04	7.6128+11	4- 5	1.3913+07	8.5036+06	1.3837+07	7.6460+04	6.6661+11
1.4092+07	8.2760+06	1.4017+07	7.5582+04	6.5695+11	5- 6	1.2829+07	7.1139+06	1.2763+07	6.6556+04	5.8062+11
1.3291+07	7.1263+06	1.3223+07	6.7837+04	6.0031+11	6- 7	1.1749+07	6.2533+06	1.1691+07	5.8423+04	5.1559+11
1.1996+07	6.1255+06	1.1940+07	5.5439+04	4.9459+11	7- 8	1.0779+07	5.4479+06	1.0729+07	4.9252+04	4.3723+11
1.0434+07	5.0579+06	1.0387+07	4.7597+04	4.1561+11	8-10	9.5210+06	4.5823+06	9.4807+06	4.0301+04	3.5080+11
9.1596+06	4.0796+06	9.1223+06	3.7331+04	3.1888+11	10-12	7.8828+06	3.4837+06	7.8519+06	3.0926+04	2.7292+11
7.8726+06	3.1447+06	7.8436+06	2.8996+04	2.5225+11	12-14	6.6574+06	2.7117+06	6.6325+06	2.4924+04	2.1779+11
6.6212+06	2.6042+06	6.5964+06	2.4756+04	2.1787+11	14-16	5.6414+06	2.2050+06	5.6223+06	1.9150+04	1.6540+11
5.6545+06	2.0444+06	5.6356+06	1.8879+04	1.6405+11	16-18	4.6340+06	1.6439+06	4.6183+06	1.5669+04	1.3575+11
4.8162+06	1.7352+06	4.7994+06	1.6809+04	1.5019+11	18-20	3.9602+06	1.3648+06	3.9470+06	1.3193+04	1.1479+11
3.9930+06	1.2294+06	3.9799+06	1.3089+04	1.1509+11	20-22	3.4469+06	1.1257+06	3.4361+06	1.0791+04	9.2734+10
3.5312+06	1.1682+06	3.5194+06	1.1826+04	9.8124+10	22-24	2.8184+06	8.7218+05	2.8093+06	9.1032+03	7.9403+10
2.8947+06	8.3294+05	2.8852+06	9.4650+03	8.3278+10	24-26	2.6030+06	8.3914+05	2.5955+06	7.5365+03	6.6243+10
2.6820+06	7.5578+05	2.6745+06	7.5284+03	6.5438+10	26-28	2.1112+06	6.1316+05	2.1052+06	5.9340+03	5.3129+10
2.0787+06	6.2138+05	2.0723+06	6.3511+03	5.4917+10	28-30	1.7964+06	4.9872+05	1.7911+06	5.3184+03	4.5402+10
1.9178+06	5.6316+05	1.9121+06	5.6248+03	4.6055+10	30-32	1.5850+06	4.7081+05	1.5807+06	4.2842+03	3.6654+10
1.5027+06	3.9034+05	1.4979+06	4.7056+03	4.1321+10	32-36	1.2711+06	3.2523+05	1.2679+06	3.1653+03	2.8001+10
1.1535+06	2.9206+05	1.1508+06	2.7422+03	2.3750+10	36-40	8.9154+05	2.1823+05	8.8915+05	2.3926+03	2.0880+10
8.3786+05	1.8361+05	8.3545+05	2.4135+03	2.1663+10	40-44	6.1179+05	1.3468+05	6.1030+05	1.4880+03	1.3035+10
5.8447+05	1.2126+05	5.8324+05	1.2239+03	1.1856+10	44-48	4.5558+05	1.0269+05	4.5440+05	1.1870+03	1.0347+10
3.6494+05	4.5690+04	3.6378+05	1.1620+03	9.6734+09	48-52	3.5304+05	7.9429+04	3.5224+05	8.0119+02	7.2991+09
4.2376+05	1.1799+05	4.2283+05	9.2341+02	7.5878+09	52-56	2.7188+05	5.8605+04	2.7120+05	6.7848+02	5.7264+09
2.0939+05	3.6548+04	2.0891+05	4.8451+02	3.9455+09	56-62	1.8377+05	3.1240+04	1.8340+05	3.7471+02	3.3093+09
1.5701+05	1.6907+04	1.5669+05	3.1657+02	3.0281+09	62-68	1.2843+05	2.1044+04	1.2815+05	2.7689+02	2.4221+09
9.0931+04	1.6137+04	9.0765+04	1.6651+02	1.4239+09	68-74	6.6194+04	8.0178+03	6.6040+04	1.5467+02	1.2540+09
5.5196+04	1.0481+04	5.5105+04	9.1451+01	7.3329+08	74-80	5.5483+04	6.4640+03	5.5377+04	1.0552+02	1.0079+09
4.7882+04	5.0886+03	4.7795+04	8.7827+01	1.0092+09	80-86	2.8577+04	3.7709+03	2.8525+04	5.2080+01	4.0987+08
3.5763+04	5.7312+03	3.5700+04	6.3494+01	6.4802+08	86-92	2.0757+04	3.2505+03	2.0723+04	3.3692+01	3.1309+08

TABLE III. TOTAL POWER GENERATION FROM NEUTRON SCATTERING BY DEPTH AND RADIAL SEGMENT NUMBER (Erg/gm-sec)

CM	0-30	30-45	45-60	60-75	75-90	90-105	105-	120.68-
0- 1	2.0285+07	2.0024+07	2.0080+07	1.9564+07	1.9134+07	1.8689+07	1.8912+07	
1- 2	1.8929+07	1.8625+07	1.8331+07	1.8186+07	1.8049+07	1.7406+07	1.7261+07	
2- 3	1.8205+07	1.7560+07	1.7159+07	1.7418+07	1.6570+07	1.6616+07	1.5430+07	
3- 4	1.6497+07	1.6654+07	1.6194+07	1.5966+07	1.5538+07	1.4866+07	1.4321+07	
4- 5	1.4943+07	1.5390+07	1.5713+07	1.4873+07	1.4346+07	1.3913+07	1.3895+07	
5- 6	1.4092+07	1.4290+07	1.4619+07	1.3260+07	1.3547+07	1.2829+07	1.2269+07	
6- 7	1.3291+07	1.3259+07	1.2677+07	1.2689+07	1.2272+07	1.1749+07	1.0483+07	
7- 8	1.1996+07	1.2167+07	1.1982+07	1.1326+07	1.1577+07	1.0779+07	9.5991+06	
8-10	1.0434+07	1.0592+07	1.0565+07	1.0209+07	1.0016+07	9.5210+06	8.2732+06	
10-12	9.1596+06	9.5410+06	8.8006+06	8.7998+06	8.4041+06	7.8828+06	6.9771+06	
12-14	7.8726+06	7.9337+06	7.8381+06	7.4540+06	7.0919+06	6.6574+06	5.8790+06	
14-16	6.6212+06	6.6847+06	6.5547+06	6.0854+06	6.0901+06	5.6414+06	4.9292+06	
16-18	5.6545+06	5.5609+06	5.2206+06	5.1937+06	5.0228+06	4.6340+06	3.7892+06	
18-20	4.8162+06	4.5177+06	4.6117+06	4.3464+06	4.2088+06	3.9602+06	3.1604+06	
20-22	3.9930+06	3.9826+06	3.9210+06	3.9055+06	3.6772+06	3.4469+06	2.7501+06	
22-24	3.5312+06	3.6151+06	3.4646+06	3.2272+06	3.1543+06	2.8184+06	2.2397+06	
24-26	2.8947+06	2.9762+06	2.8957+06	2.6529+06	2.6198+06	2.6030+06	1.8746+06	
26-28	2.6820+06	2.4242+06	2.4097+06	2.3797+06	2.2324+06	2.1112+06	1.5717+06	
28-30	2.0787+06	2.0314+06	2.0697+06	2.1375+06	1.9412+06	1.7964+06	1.4687+06	
30-32	1.9178+06	1.8916+06	1.7113+06	1.6730+06	1.7312+06	1.5850+06	1.2302+06	
32-36	1.5027+06	1.4846+06	1.3593+06	1.3774+06	1.2716+06	1.2711+06	9.4544+05	
36-40	1.1535+06	1.0814+06	1.0609+06	9.9807+05	9.5317+05	8.9154+05	7.2848+05	
40-44	8.3786+05	7.7671+05	7.1183+05	7.3031+05	6 8642+05	6.1179+05	5.1596+05	2.9229+05
44-48	5.8447+05	5.8951+05	6.1117+05	5.2285+05	5.2163+05	4.5558+05	3.7668+05	2.8027+05
48-52	3.6494+05	4.6847+05	3.9085+05	3.8193+05	3.7510+05	3.5304+05	2.7781+05	1.9296+05
52-56	4.2376+05	3.4903+05	3.6481+05	2.8951+05	3.1703+05	2.7188+05	2.4264+05	1.2565+05
56-62	2.0939+05	2.1216+05	2.2111+05	1.9821+05	1.8849+05	1.8377+05	1.8079+05	9.8318+04
62-68	1.5701+05	1.1346+05	1.3742+05	1.1944+05	1.3271+05	1.2843+05	1.0223+05	7.2109+04
68-74	9.0931+04	8.6637+04	1.0449+05	8.4519+04	1.0497+05	6.6194+04	6.5566+04	4.5130+04
74-80	5.5196+04	4.4850+04	6.3163+04	5.8411+04	8.3091+04	5.5483+04	3.8740+04	2.6029+04
80-86	4.7882+04	4.3391+04	6.1136+04	3.6581+04	4.6657+04	2.8577+04	3.2570+04	1.9531+04
86-92	3.5763+04	2.6579+04	2.8342+04	1.9960+04	2.7992+04	2.0757+04	2.2558+04	1.8391+04

TABLE IV. SCATTERING POWER GENERATION FROM GROUP 1 BY DEPTH AND RADIUS (Erg/gm-sec)

CM	0-30	30-45	45-60	60-75	75-90	90-105	105-	120.68-
0- 1	4.2978+06	4.1774+06	4.5779+06	4.1133+06	4.1002+06	3.9982+06	3.8435+06	
1- 2	4.0881+06	3.9009+06	3.9921+06	3.7758+06	3.9161+06	3.7564+06	3.6244+06	
2- 3	3.7518+06	3.7720+06	4.1033+06	3.8690+06	3.6836+06	3.8865+06	3.8174+06	
3- 4	3.7163+06	3.9140+06	4.3434+06	3.6550+06	3.7874+06	3.3114+06	3.7067+06	
4- 5	3.8999+06	3.5740+06	3.8551+06	3.8474+06	3.5722+06	3.5301+06	3.6816+06	
5- 6	3.8324+06	4.0424+06	3.8692+06	3.3656+06	3.5670+06	3.2997+06	3.4825+06	
6- 7	3.4496+06	3.6746+06	3.3292+06	3.5187+06	3.3161+06	3.2853+06	2.9850+06	
7- 8	3.6123+06	3.6749+06	3.5675+06	3.1706+06	3.4036+06	3.2415+06	2.6868+06	
8-10	3.2389+06	3.1713+06	3.4099+06	3.2110+06	3.0235+06	2.9844+06	2.6483+06	
10-12	3.0533+06	3.1872+06	2.9933+06	3.0718+06	2.8230+06	2.7443+06	2.3338+06	
12-14	2.7977+06	2.7305+06	2.8182+06	2.7292+06	2.5361+06	2.3720+06	2.2419+06	
14-16	2.4256+06	2.6288+06	2.5090+06	2.3114+06	2.4337+06	2.1926+06	2.0680+06	
16-18	2.5075+06	2.3202+06	2.1040+06	2.0299+06	2.0913+06	1.8975+06	1.6721+06	
18-20	2.1458+06	1.9270+06	1.9648+06	1.9771+06	1.7546+06	1.7496+06	1.4519+06	
20-22	1.6776+06	1.8053+06	1.7846+06	1.7621+06	1.6897+06	1.5617+06	1.3305+06	
22-24	1.6731+06	1.6371+06	1.6021+06	1.5765+06	1.5277+06	1.3654+06	1.0947+06	
24-26	1.5347+06	1.4278+06	1.4602+06	1.3282+06	1.2162+06	1.3573+06	9.7953+05	
26-28	1.3856+06	1.2878+06	1.2753+06	1.2284+06	1.1880+06	1.1297+06	8.3295+05	
28-30	1.0818+06	1.0035+06	1.0917+06	1.1360+06	1.0583+06	1.0308+06	8.5046+05	
30-32	1.1538+06	1.1011+06	9.4489+05	9.7864+05	1.0150+06	8.7945+05	7.2200+05	
32-36	8.7870+05	8.8062+05	8.2957+05	8.2556+05	7.8658+05	7.6159+05	5.8157+05	
36-40	6.8807+05	7.3136+05	6.4994+05	6.4522+05	6.0007+05	5.9532+05	4.7684+05	
40-44	5.2625+05	5.1843+05	4.4362+05	5.0494+05	4.7019+05	4.3089+05	3.4041+05	2.0246+05
44-48	4.2746+05	4.4003+05	4.3330+05	3.6630+05	3.8726+05	3.3642+05	2.6832+05	2.1976+05
48-52	2.6571+05	3.2035+05	3.0221+05	2.6524+05	2.9989+05	2.6269+05	2.1848+05	1.6433+05
52-56	3.3815+05	2.4636+05	2.7038+05	2.2125+05	2.4804+05	2.3100+05	1.9928+05	1.0120+05
56-62	1.7214+05	1.6862+05	1.7388+05	1.6963+05	1.5444+05	1.5277+05	1.5370+05	8.9394+04
62-68	1.4111+05	9.4474+04	1.1801+05	1.0148+05	1.1308+05	1.1215+05	8.5406+04	6.1859+04
68-74	8.6352+04	7.9319+04	9.1730+04	7.0538+04	9.6935+04	5.8171+04	5.7570+04	3.9147+04
74-80	4.8259+04	4.1119+04	5.6881+04	5.2053+04	7.4697+04	4.9938+04	3.6239+04	2.4486+04
80-86	4.2566+04	4.0956+04	5.7195+04	3.3499+04	4.4249+04	2.6356+04	3.0981+04	1.8586+04
86-92	3.4297+04	2.6579+04	2.8177+04	1.6204+04	2.6316+04	1.9185+04	2.1958+04	1.7060+04

TABLE V. SCATTERING POWER GENERATION FROM GROUP 2 BY DEPTH AND RADIUS (Erg/gm-sec)

CM	0-30	30-45	45-60	60-75	75-90	90-105	105-	120.68-
0- 1	6.7935+06	6.7540+06	6.3377+06	6.3371+06	6.4439+06	6.3032+06	6.9496+06	
1- 2	6.4499+06	6.3595+06	6.2225+06	6.2616+06	6.2525+06	6.1807+06	6.3899+06	
2- 3	6.7960+06	6.3054+06	5.8710+06	6.2182+06	6.0164+06	5.9428+06	5.4993+06	
3- 4	6.2058+06	6.2580+06	5.3836+06	5.8912+06	5.6457+06	5.5632+06	4.9517+06	
4- 5	5.4264+06	5.9929+06	6.1005+06	5.5629+06	5.4473+06	5.2549+06	5.6074+06	
5- 6	5.3963+06	5.4892+06	5.8771+06	5.1507+06	5.2541+06	5.0374+06	4.8499+06	
6- 7	5.5258+06	5.2725+06	5.0431+06	5.0918+06	4.8436+06	4.6251+06	4.1040+06	
7- 8	4.6843+06	4.9811+06	4.8173+06	4.6402+06	4.6984+06	4.2401+06	4.0531+06	
8-10	4.1743+06	4.3991+06	4.2893+06	4.1379+06	4.2318+06	3.9258+06	3.4361+06	
10-12	3.8531+06	4.2009+06	3.7414+06	3.6201+06	3.6383+06	3.2447+06	3.0231+06	
12-14	3.3831+06	3.5999+06	3.3855+06	3.1795+06	3.0508+06	2.9174+06	2.5827+06	
14-16	2.8200+06	2.8377+06	2.7507+06	2.6826+06	2.5627+06	2.4556+06	2.0441+06	
16-18	2.2348+06	2.3019+06	2.2446+06	2.3465+06	2.1383+06	2.0115+06	1.5562+06	
18-20	2.0192+06	1.9516+06	1.9958+06	1.8005+06	1.8599+06	1.6725+06	1.2496+06	
20-22	1.8217+06	1.6755+06	1.6309+06	1.7028+06	1.5462+06	1.4671+06	1.1030+06	
22-24	1.5091+06	1.5911+06	1.4748+06	1.3165+06	1.3075+06	1.1640+06	9.1363+05	
24-26	1.0816+06	1.2989+06	1.1658+06	1.1026+06	1.1591+06	1.0207+06	7.2396+05	
26-28	1.0713+06	9.4329+05	9.5126+05	9.6706+05	8.6526+05	8.0771+05	6.3610+05	
28-30	8.4184+05	8.7221+05	8.4295+05	8.5188+05	7.3262+05	6.4638+05	5.2642+05	
30-32	6.6252+05	6.7231+05	6.5569+05	5.9507+05	6.1576+05	6.1077+05	4.4462+05	
32-36	5.6948+05	5.3292+05	4.7136+05	4.8956+05	4.2360+05	4.4354+05	3.2066+05	
36-40	4.3422+05	3.1352+05	3.6445+05	3.1055+05	3.2200+05	2.7041+05	2.3122+05	
40-44	2.8990+05	2.3538+05	2.4679+05	2.0313+05	2.0021+05	1.7075+05	1.6570+05	8.3764+04
44-48	1.4755+05	1.3639+05	1.6952+05	1.4643+05	1.2770+05	1.1188+05	1.0185+05	5.9585+04
48-52	8.9892+04	1.3952+05	8.2025+04	1.0673+05	7.1698+04	8.5967+04	5.3583+04	2.6291+04
52-56	7.9589+04	9.6775+04	9.1327+04	6.4255+04	6.6041+04	3.8803+04	3.9432+04	2.4252+04
56-62	3.2135+04	4.2069+04	4.4759+04	2.7803+04	3.2655+04	2.9776+04	2.6753+04	8.7350+03
62-68	1.5882+04	1.7998+04	1.8043+04	1.7607+04	1.9015+04	1.5178+04	1.6536+04	1.0228+04
68-74	4.5792+03	7.2135+03	1.2425+04	1.3135+04	7.4293+03	7.8216+03	7.8503+03	5.9826+03
74-80	6.9370+03	3.7312+03	5.9658+03	5.2144+03	8.0519+03	5.3113+03	2.5014+03	1.5427+03
80-86	5.3164+03	2.4351+03	3.9411+03	3.0820+03	2.4087+03	2.0226+03	1.5892+03	9.4431+02
86-92	1.4662+03	0.0000+00	1.6438+02	3.7557+03	1.6767+03	1.4905+03	5.9945+02	1.3315+03

TABLE VI. SCATTERING POWER GENERATION FROM GROUP 3 BY DEPTH AND RADIUS (Erg/gm-sec)

CM	0-30	30-45	45-60	60-75	75-90	90-105	105-	120.68-
0- 1	2.8203+06	2.9187+06	2.8617+06	2.9263+06	2.6735+06	2.6884+06	2.4528+06	
1- 2	2.7065+06	2.8259+06	2.6163+06	2.6871+06	2.6609+06	2.4115+06	2.4783+06	
2- 3	2.8032+06	2.4498+06	2.4242+06	2.6591+06	2.2796+06	2.3470+06	2.2423+06	
3- 4	2.4866+06	2.3455+06	2.4247+06	2.4291+06	2.2340+06	2.3091+06	2.5149+06	
4- 5	2.1716+06	2.3909+06	2.2702+06	2.2040+06	2.0727+06	2.0805+06	1.8896+06	
5- 6	1.8685+06	2.0133+06	2.1576+06	2.0273+06	2.0248+06	1.9419+06	1.6936+06	
6- 7	1.9101+06	1.8749+06	1.9076+06	1.8040+06	1.7389+06	1.6919+06	1.4761+06	
7- 8	1.7426+06	1.6929+06	1.6585+06	1.5805+06	1.6207+06	1.5846+06	1.3224+06	
8-10	1.5081+06	1.5650+06	1.3862+06	1.3863+06	1.3671+06	1.3229+06	1.1791+06	
10-12	1.2345+06	1.1365+06	1.0451+06	1.1008+06	9.8544+05	1.0385+06	8.9929+05	
12-14	9.7411+05	9.1419+05	9.1856+05	8.7889+05	8.1513+05	7.7922+05	6.0502+05	
14-16	8.0173+05	6.8819+05	7.7067+05	6.6823+05	6.4886+05	6.2547+05	4.9559+05	
16-18	6.0151+05	5.7125+05	5.6648+05	5.0463+05	5.0118+05	4.5744+05	3.7339+05	
18-20	4.4749+05	3.9882+05	4.3375+05	3.5600+05	3.8979+05	3.6672+05	3.2129+05	
20-22	3.4770+05	3.5588+05	3.4087+05	2.9796+05	3.1057+05	3.0079+05	2.3109+05	
22-24	2.4633+05	2.7051+05	2.7278+05	2.3999+05	2.1329+05	2.0359+05	1.6767+05	
24-26	2.1064+05	1.6714+05	1.8995+05	1.6084+05	1.8471+05	1.6706+05	1.2028+05	
26-28	1.6143+05	1.3307+05	1.3113+05	1.3726+05	1.4021+05	1.3556+05	8.4792+04	
28-30	1.2368+05	1.2539+05	1.1779+05	1.1192+05	1.1882+05	9.1043+04	7.1489+04	
30-32	8.2651+04	9.4350+04	8.9521+04	8.1636+04	7.9896+04	7.4246+04	5.2732+04	
32-36	4.4038+04	5.5689+04	5.0094+04	4.9565+04	4.9111+04	5.0022+04	3.7284+04	
36-40	2.9405+04	3.0358+04	3.6441+04	3.5677+04	2.6119+04	2.1207+04	1.8890+04	
40-44	2.1083+04	2.0053+04	1.8876+04	1.7860+04	1.5139+04	9.1905+03	8.9468+03	6.0717+03
44-48	9.4537+03	1.2112+04	6.5750+03	7.8917+03	5.4374+03	6.4368+03	6.2793+03	9.2789+02
48-52	8.0828+03	7.8713+03	5.8361+03	8.5424+03	2.1978+03	4.0524+03	5.7184+03	2.3331+03
52-56	5.9368+03	5.8604+03	3.1049+03	3.7311+03	1.9935+03	1.4275+03	3.9215+03	1.9886+02
56-62	5.1185+03	1.4768+03	2.4751+03	7.4192+02	1.3975+03	1.2215+03	3.2947+02	1.8906+02
62-68	2.1669+01	9.9196+02	6.2868+02	3.5318+02	6.1300+02	9.1679+02	2.1292+02	2.2475+01
68-74	0.0000+00	1.0468+02	2.3740+02	8.4571+02	6.0254+02	2.0213+02	1.4494+02	0.0000+00
74-80	0.0000+00	0.0000+00	3.1555+02	1.1429+03	3.4203+02	2.3320+02	0.0000+00	0.0000+00
80-86	0.0000+00	0.0000+00	0.0000+00	0.0000+00	0.0000+00	1.9881+02	0.0000+00	0.0000+00
86-92	0.0000+00	0.0000+00	0.0000+00	0.0000+00	0.0000+00	8.1917+01	0.0000+00	0.0000+00

TABLE VII. SCATTERING POWER GENERATION FROM GROUP 4 BY DEPTH AND RADIUS (Erg/gm-sec)

CM	0-30	30-45	45-60	60-75	75-90	90-105	105-	120.68-
0- 1	3.2371+06	3.1779+06	3.1690+06	3.1177+06	2.9477+06	2.8220+06	2.8193+06	
1- 2	3.0004+06	2.8677+06	2.8645+06	2.8759+06	2.6986+06	2.6463+06	2.4916+06	
2- 3	2.6994+06	2.8653+06	2.6730+06	2.5581+06	2.5745+06	2.4811+06	2.2712+06	
3- 4	2.2953+06	2.5164+06	2.2815+06	2.4039+06	2.2901+06	2.1596+06	1.8731+06	
4- 5	2.1484+06	2.1546+06	2.1875+06	2.0088+06	1.9855+06	1.9118+06	1.6734+06	
5- 6	2.0114+06	1.7203+06	1.7603+06	1.7778+06	1.7763+06	1.6952+06	1.5310+06	
6- 7	1.6903+06	1.6594+06	1.5949+06	1.5410+06	1.6240+06	1.4565+06	1.3494+06	
7- 8	1.3583+06	1.2720+06	1.3715+06	1.3735+06	1.3307+06	1.2289+06	1.0474+06	
8-10	1.1081+06	1.0666+06	1.0996+06	1.1021+06	1.0553+06	9.6884+05	7.7057+05	
10-12	8.0498+05	7.9608+05	8.1210+05	7.8950+05	7.5016+05	6.6243+05	5.5110+05	
12-14	6.0121+05	5.7350+05	5.8322+05	5.5116+05	5.8365+05	4.8659+05	3.7407+05	
14-16	4.9568+05	4.5406+05	4.4713+05	3.5243+05	3.8384+05	3.1555+05	2.8425+05	
16-18	2.7703+05	3.2950+05	2.7335+05	2.7726+05	2.5883+05	2.3849+05	1.6238+05	
18-20	1.7383+05	2.1623+05	1.9468+05	1.8939+05	1.8454+05	1.5187+05	1.2922+05	
20-22	1.3395+05	1.3373+05	1.4845+05	1.2747+05	1.2074+05	1.0760+05	8.2272+04	
22-24	9.7604+04	1.0816+05	1.0404+05	8.8072+04	1.0060+05	8.1549+04	6.0281+04	
24-26	5.9771+04	8.0290+04	7.7491+04	5.8814+04	5.6476+04	5.5801+04	5.0050+04	
26-28	5.8924+04	5.7137+04	4.9968+04	4.2601+04	3.6726+04	3.6604+04	1.6988+04	
28-30	2.9332+04	3.0253+04	1.6969+04	3.7534+04	3.1026+04	2.7147+04	1.9396+04	
30-32	1.8720+04	2.3807+04	2.0684+04	1.6598+04	1.9513+04	1.9680+04	1.0364+04	
32-36	1.0071+04	1.5340+04	8.2435+03	1.2445+04	1.2035+04	1.5047+04	5.8344+03	
36-40	1.8283+03	6.1130+03	9.9751+03	6.6227+03	4.9787+03	4.6070+03	1.4246+03	
40-44	6.3093+02	2.8420+03	2.5388+03	4.3902+03	8.7273+02	9.6226+02	9.0264+02	0.0000+00
44-48	0.0000+00	9.7232+02	1.7790+03	2.2330+03	1.2356+03	8.4756+02	2.3692+02	0.0000+00
48-52	1.2555+03	7.2797+02	7.7654+02	1.4160+03	1.3126+03	3.3133+02	2.7477+01	0.0000+00
52-56	8.1058+01	3.2338+01	0.0000+00	2.7978+02	9.5962+02	6.4669+02	0.0000+00	0.0000+00
56-62	0.0000+00	0.0000+00	0.0000+00	3.8932+01	0.0000+00	0.0000+00	0.0000+00	0.0000+00
62-68	0.0000+00	0.0000+00	7.4416+02	0.0000+00	0.0000+00	1.8182+02	7.9640+01	0.0000+00
68-74	0.0000+00	0.0000+00	9.5213+01	0.0000+00	0.0000+00	0.0000+00	0.0000+00	0.0000+00
74-80	0.0000+00	0.0000+00	0.0000+00	0.0000+00	0.0000+00	0.0000+00	0.0000+00	0.0000+00
80-86	0.0000+00	0.0000+00	0.0000+00	0.0000+00	0.0000+00	0.0000+00	0.0000+00	0.0000+00
86-92	0.0000+00	0.0000+00	0.0000+00	0.0000+00	0.0000+00	0.0000+00	0.0000+00	0.0000+00

TABLE VIII. SCATTERING POWER GENERATION FROM GROUP 5 BY DEPTH AND RADIUS (Erg/gm-sec)

CM	0-30	30-45	45-60	60-75	75-90	90-105	105-	120.68-
0- 1	2.3256+06	2.2515+06	2.3559+06	2.3237+06	2.2533+06	2.1566+06	2.1733+06	
1- 2	2.0826+06	2.0947+06	2.0507+06	2.0229+06	1.9754+06	1.8838+06	1.8015+06	
2- 3	1.7609+06	1.7634+06	1.6908+06	1.7083+06	1.6363+06	1.5848+06	1.2542+06	
3- 4	1.5053+06	1.3528+06	1.4771+06	1.3301+06	1.3189+06	1.2827+06	1.0714+06	
4- 5	1.1034+06	1.0915+06	1.1184+06	1.0779+06	1.1062+06	9.8311+05	9.1575+05	
5- 6	8.5169+05	9.0497+05	8.3943+05	8.2243+05	8.2227+05	7.5087+05	6.4002+05	
6- 7	6.4489+05	7.1169+05	7.3596+05	6.5782+05	6.8265+05	6.3218+05	5.2743+05	
7- 8	5.5941+05	5.0319+05	5.1912+05	5.1568+05	4.8173+05	4.4378+05	4.6215+05	
8-10	3.8046+05	3.6314+05	3.5942+05	3.4704+05	3.1916+05	3.0117+05	2.2694+05	
10-12	2.0404+05	2.0901+05	2.0177+05	2.0917+05	1.9898+05	1.8571+05	1.6422+05	
12-14	1.1366+05	1.1222+05	1.2927+05	1.1315+05	1.0363+05	9.9800+04	7.3205+04	
14-16	7.6509+04	7.4939+04	7.5332+04	6.8867+04	5.9704+04	5.1459+04	3.6653+04	
16-18	3.2863+04	3.7096+04	3.2028+04	3.4705+04	3.2867+04	2.8730+04	2.4657+04	
18-20	2.9780+04	2.2933+04	2.2625+04	2.3250+04	1.9871+04	1.9473+04	8.3769+03	
20-22	1.1920+04	1.1962+04	1.6050+04	1.5074+04	1.0054+04	9.5700+03	3.1821+03	
22-24	5.0706+03	8.3221+03	1.0809+04	6.1570+03	5.2566+03	3.8772+03	3.3791+03	
24-26	7.9912+03	2.0374+03	2.3271+03	2.4927+03	3.3713+03	2.1729+03	8.1651+02	
26-28	4.7539+03	2.9461+03	2.1214+03	4.3672+03	2.2704+03	1.5077+03	8.4222+02	
28-30	2.0044+03	2.6408-01	2.9404+02	1.0358+02	4.5398+02	1.0316+03	9.4618+02	
30-32	5.0614+01	0.0000+00	4.9567+02	1.1033+03	1.0611+03	8.2306+02	4.9238+02	
32-36	3.5920+02	4.2115+01	7.5450-01	3.1852+02	2.5115+02	9.0785+02	9.4291+01	
36-40	0.0000+00	0.0000+00	9.6349+01	0.0000+00	0.0000+00	0.0000+00	1.0070+02	
40-44	0.0000+00	0.0000+00	0.0000+00	0.0000+00	0.0000+00	0.0000+00	0.0000+00	0.0000+00
44-48	0.0000+00	0.0000+00	0.0000+00	0.0000+00	0.0000+00	0.0000+00	0.0000+00	0.0000+00
48-52	0.0000+00	0.0000+00	0.0000+00	0.0000+00	0.0000+00	0.0000+00	0.0000+00	0.0000+00
52-56	0.0000+00	0.0000+00	0.0000+00	0.0000+00	0.0000+00	0.0000+00	0.0000+00	0.0000+00
56-62	0.0000+00	0.0000+00	0.0000+00	0.0000+00	0.0000+00	0.0000+00	0.0000+00	0.0000+00
62-68	0.0000+00	0.0000+00	0.0000+00	0.0000+00	0.0000+00	0.0000+00	0.0000+00	0.0000+00
68-74	0.0000+00	0.0000+00	0.0000+00	0.0000+00	0.0000+00	0.0000+00	0.0000+00	0.0000+00
74-80	0.0000+00	0.0000+00	0.0000+00	0.0000+00	0.0000+00	0.0000+00	0.0000+00	0.0000+00
80-86	0.0000+00	0.0000+00	0.0000+00	0.0000+00	0.0000+00	0.0000+00	0.0000+00	0.0000+00
86-92	0.0000+00	0.0000+00	0.0000+00	0.0000+00	0.0000+00	0.0000+00	0.0000+00	0.0000+00

TABLE IX. SCATTERING POWER GENERATION FROM GROUP 6 BY DEPTH AND RADIUS (Erg/gm-sec)

CM	0-30	30-45	45-60	60-75	75-90	90-105	105-	120.68-
0- 1	8.1084+05	7.4434+05	7.7773+05	7.4614+05	7.1502+05	7.2033+05	6.7336+05	
1- 2	6.0110+05	5.7652+05	5.8490+05	5.6292+05	5.4583+05	5.2751+05	4.7552+05	
2- 3	3.9413+05	4.0360+05	3.9635+05	4.0487+05	3.7947+05	3.7417+05	3.4578+05	
3- 4	2.8804+05	2.6719+05	2.8322+05	2.5701+05	2.6171+05	2.3985+05	2.0291+05	
4- 5	1.9308+05	1.8638+05	1.8158+05	1.7152+05	1.6224+05	1.5260+05	1.2705+05	
5- 6	1.3185+05	1.1984+05	1.1508+05	1.1572+05	1.0236+05	1.0413+05	7.2479+04	
6- 7	7.0698+04	6.5615+04	6.6021+04	7.5772+04	6.6269+04	5.8155+04	4.1504+04	
7- 8	3.8963+04	4.3039+04	4.8132+04	4.5030+04	4.1807+04	3.9972+04	2.7214+04	
8-10	2.4323+04	2.6840+04	2.0290+04	2.4664+04	1.8840+04	1.7963+04	1.2146+04	
10-12	9.8149+03	1.1296+04	6.9723+03	8.3689+03	8.2675+03	7.1158+03	5.7076+03	
12-14	2.7688+03	3.3585+03	3.4161+03	2.1344+03	2.5962+03	2.4282+03	2.1589+03	
14-16	1.6602+03	9.7960+02	1.8956+03	1.8165+03	1.3462+03	7.4470+02	5.9314+02	
16-18	7.7122+02	9.5191+02	1.2795+02	7.0088+02	2.8358+02	2.9445+02	5.2065+02	
18-20	1.3109+02	1.1168+03	5.5665+01	8.0581+01	1.1946+02	4.7400+01	0.0000+00	
20-22	0.0000+00	1.8331+02	1.6562+02	8.0702+01	0.0000-00	1.8302+02	3.5106+01	
22-24	0.0000+00	0.0000+00	0.0000+00	0.0000+00	0.0000+00	2.4158+01	7.0194+01	
24-26	0.0000+00	0.0000+00	0.0000+00	0.0000+00	0.0000+00	0.0000+00	0.0000+00	
26-28	0.0000+00	0.0000+00	0.0000+00	0.0000+00	0.0000+00	1.3066+02	0.0000+00	
28-30	0.0000+00	0.0000+00	0.0000+00	0.0000+00	0.0000+00	6.4231+01	0.0000+00	
30-32	0.0000+00	0.0000+00	0.0000+00	0.0000+00	0.0000+00	0.0000+00	0.0000+00	
32-36	0.0000+00	0.0000+00	0.0000+00	0.0000+00	0.0000+00	0.0000+00	0.0000+00	
36-40	0.0000+00	0.0000+00	0.0000+00	0.0000+00	0.0000+00	0.0000+00	0.0000+00	
40-44	0.0000+00	0.0000+00	0.0000+00	0.0000+00	0.0000+00	0.0000+00	0.0000+00	0.0000+00
44 48	0.0000+00	0.0000+00	0.0000+00	0.0000+00	0.0000+00	0.0000+00	0.0000+00	0.0000+00
48-52	0.0000+00	0.0000+00	0.0000+00	0.0000+00	0.0000+00	0.0000+00	0.0000+00	0.0000+00
52-56	0.0000+00	0.0000+00	0.0000+00	0.0000+00	0.0000+00	0.0000+00	0.0000+00	0.0000+00
56-62	0.0000+00	0.0000+00	0.0000+00	0.0000+00	0.0000+00	0.0000+00	0.0000+00	0.0000+00
62-68	0.0000+00	0.0000+00	0.0000+00	0.0000+00	0.0000+00	0.0000+00	0.0000+00	0.0000+00
68-74	0.0000+00	0.0000+00	0.0000+00	0.0000+00	0.0000+00	0.0000+00	0.0000+00	0.0000+00
74-80	0.0000+00	0.0000+00	0.0000+00	0.0000+00	0.0000+00	0.0000+00	0.0000+00	0.0000+00
80-86	0.0000+00	0.0000+00	0.0000+00	0.0000+00	0.0000+00	0.0000+00	0.0000+00	0.0000+00
86-92	0.0000+00	0.0000+00	0.0000+00	0.0000+00	0.0000+00	0.0000+00	0.0000+00	0.0000+00

TABLE X. INNER NEUTRON SCATTERING POWER GENERATION BY DEPTH AND RADIUS (Erg/gm-sec)

CM	0-30	30-45	45-60	60-75	75-90	90-105	105-	120.68-
0- 1	2.0285+07	2.0024+07	2.0080+07	1.9543+07	1.5556+05	3.4386+03	5.9112+02	
1- 2	1.8929+07	1.8625+07	1.8331+07	1.8142+07	5.3227+05	4.8633+03	4.2399+03	
2- 3	1.8205+07	1.7560+07	1.7158+07	1.7346+07	8.6192+05	3.9524+03	0.0000+00	
3- 4	1.6497+07	1.6654+07	1.6193+07	1.5870+07	1.0196+06	5.1602+03	5.1266+01	
4- 5	1.4943+07	1.5390+07	1.5711+07	1.4750+07	1.1899+06	4.2386+03	5.4238+03	
5- 6	1.4092+07	1.4290+07	1.4618+07	1.3121+07	1.4740+06	9.5938+03	7.4002+03	
6- 7	1.3291+07	1.3259+07	1.2677+07	1.2535+07	1.3408+06	1.2070+04	3.3058+03	
7- 8	1.1996+07	1.2167+07	1.1981+07	1.1160+07	1.4989+06	1.8421+04	1.9412+03	
8-10	1.0434+07	1.0592+07	1.0563+07	1.0051+07	1.5986+06	1.7472+04	4.5191+01	
10-12	9.1596+06	9.5408+06	8.7995+06	8.6478+06	1.6815+06	2.0087+04	1.9834+03	
12-14	7.8726+06	7.9330+06	7.8360+06	7.2800+06	1.6488+06	2.3554+04	1.5976+03	
14-16	6.6212+06	6.6847+06	6.5525+06	5.9071+06	1.6391+06	3.3974+04	6.3044+03	
16-18	5.6545+06	5.5609+06	5.2187+06	5.0170+06	1.3381+06	4.5045+04	2.4277+03	
18-20	4.8162+06	4.5177+06	4.6085+06	4.1871+06	1.2919+06	2.8663+04	3.4358+03	
20-22	3.9930+06	3.9826+06	3.9175+06	3.7578+06	1.2903+06	4.5588+04	5.8919+03	
22-24	3.5312+06	3.6131+06	3.4596+06	3.0966+06	1.1526+06	3.6731+04	1.7023+03	
24-26	2.8947+06	2.9762+06	2.8916+06	2.5395+06	9.5603+05	5.2908+04	1.1713+04	
26-28	2.6820+06	2.4234+06	2.4024+06	2.2827+06	9.3654+05	5.8602+04	5.2547+03	
28-30	2.0787+06	2.0312+06	2.0643+06	2.0292+06	8.3062+05	6.2964+04	1.3401+04	
30-32	1.9178+06	1.8916+06	1.7077+06	1.5792+06	7.8574+05	7.2858+04	7.4244+03	
32-36	1.5027+06	1.4845+06	1.3500+06	1.3035+06	6.2669+05	5.2401+04	4.5552+03	
36-40	1.1535+06	1.0799+06	1.0557+06	9.4102+05	5.3176+05	5.8531+04	1.0022+04	
40-44	8.3786+05	7.7594+05	7.0692+05	6.7109+05	4.0036+05	4.3082+04	6.3296+03	0.0000+00
44-48	5.8447+05	5.8951+05	6.0595+05	4.8621+05	3.0275+05	4.1001+04	6.9902+03	7.6249+03
48-52	3.6494+05	4.6847+05	3.8676+05	3.4024+05	2.5445+05	4.0662+04	3.8683+03	9.4637+03
52-56	4.2376+05	3.4903+05	3.6203+05	2.7043+05	2.0456+05	2.7405+04	7.1012+03	3.1677+03
56-62	2.0939+05	2.1138+05	2.1960+05	1.8234+05	1.3489+05	2.8265+04	7.3458+03	2.5874+01
62-68	1.5701+05	1.1265+05	1.3335+05	1.1078+05	9.7225+04	2.4567+04	4.3720+03	7.4785+02
68-74	9.0931+04	8.6637+04	1.0179+05	8.1074+04	7.8846+04	1.4199+04	4.8857+03	1.2820+03
74-80	5.5196+04	4.4850+04	6.0459+04	5.4640+04	6.4447+04	2.1663+04	1.3675+03	8.7318+02
80-86	4.7882+04	4.2118+04	6.0154+04	3.3236+04	3.4036+04	1.1148+04	2.3285+03	8.4519+02
86-92	3.5763+04	2.6579+04	2.6622+04	1.9225+04	2.2987+04	6.7486+03	2.3642+03	3.4799+02

TABLE XI. OUTER NEUTRON SCATTERING POWER GENERATION BY DEPTH AND RADIUS (Erg/gm-sec)

CM	0-30	30-45	45-60	60-75	75-90	90-105	105-	120.68-
0- 1	0.0000+00	0.0000+00	0.0000+00	2.0768+04	1.8978+07	1.8685+07	1.8911+07	
1- 2	0.0000+00	0.0000+00	1.6365+02	4.3977+04	1.7517+07	1.7401+07	1.7257+07	
2- 3	0.0000+00	0.0000+00	4.5020+02	7.1214+04	1.5708+07	1.6612+07	1.5430+07	
3- 4	0.0000+00	0.0000+00	1.3757+02	9.5912+04	1.4518+07	1.4861+07	1.4321+07	
4- 5	0.0000+00	0.0000+00	2.0834+03	1.2252+05	1.3156+07	1.3909+07	1.3889+07	
5- 6	0.0000+00	0.0000+00	5.0715+02	1.3904+05	1.2073+07	1.2820+07	1.2262+07	
6- 7	0.0000+00	0.0000+00	1.5507+02	1.5365+05	1.0931+07	1.1737+07	1.0480+07	
7- 8	0.0000+00	0.0000+00	1.0537+03	1.6569+05	1.0078+07	1.0760+07	9.5971+06	
8-10	0.0000+00	0.0000+00	1.2341+03	1.5800+05	8.4171+06	9.5035+06	8.2731+06	
10-12	0.0000+00	1.7003+02	1.1064+03	1.5199+05	6.7226+06	7.8627+06	6.9752+06	
12-14	0.0000+00	7.2975+02	2.1210+03	1.7406+05	5.4431+06	6.6339+06	5.8774+06	
14-16	0.0000+00	0.0000+00	2.2006+03	1.7827+05	4.4511+06	5.6074+06	4.9229+06	
16-18	0.0000+00	0.0000+00	1.9237+03	1.7663+05	3.6847+06	4.5889+06	3.7868+06	
18-20	0.0000+00	0.0000+00	3.2339+03	1.5926+05	2.9170+06	3.9315+06	3.1570+06	
20-22	0.0000+00	0.0000+00	3.4466+03	1.4762+05	2.3870+06	3.4013+06	2.7442+06	
22-24	0.0000+00	2.0263+03	4.9659+03	1.3059+05	2.0018+06	2.7817+06	2.2380+06	
24-26	0.0000+00	0.0000+00	4.1101+03	1.1347+05	1.6638+06	2.5501+06	1.8629+06	
26-28	0.0000+00	7.9452+02	7.3689+03	9.6991+04	1.2959+06	2.0526+06	1.5664+06	
28-30	0.0000+00	2.0939+02	5.4308+03	1.0831+05	1.1106+06	1.7335+06	1.4553+06	
30-32	0.0000+00	0.0000+00	3.6162+03	9.3875+04	9.4549+05	1.5121+06	1.2228+06	
32-36	0.0000+00	7.1332+01	9.2751+03	7.3925+04	6.4490+05	1.2187+06	9.4089+05	
36-40	0.0000+00	1.4163+03	5.2188+03	5.7051+04	4.2141+05	8.3301+05	7.1845+05	
40-44	0.0000+00	7.6825+02	4.9108+03	5.9224+04	2.8606+05	5.6871+05	5.0963+05	2.9229+05
44-48	0.0000+00	0.0000+00	5.2250+03	3.6646+04	2.1888+05	4.1458+05	3.6969+05	2.7265+05
48-52	0.0000+00	0.0000+00	4.0847+03	4.1689+04	1.2065+05	3.1238+05	2.7394+05	1.8349+05
52-56	0.0000+00	0.0000+00	2.7833+03	1.9081+04	1.1248+05	2.4447+05	2.3553+05	1.2248+05
56-62	0.0000+00	7.7653+02	1.5049+03	1.5872+04	5.3599+04	1.5551+05	1.7344+05	9.8292+04
62-68	0.0000+00	8.1815+02	4.0735+03	8.6639+03	3.5481+04	1.0386+05	9.7863+04	7.1362+04
68-74	0.0000+00	0.0000+00	2.6945+03	3.4445+03	2.6121+04	5.1996+04	6.0680+04	4.3848+04
74-80	0.0000+00	0.0000+00	2.7036+03	3.7707+03	1.8644+04	3.3819+04	3.7372+04	2.5156+04
80-86	0.0000+00	1.2732+03	9.8142+02	3.3456+03	1.2622+04	1.7429+04	3.0241+04	1.8685+04
86-92	0.0000+00	0.0000+00	1.7193+03	7.3517+02	5.0052+03	1.4008+04	2.0193+04	1.8043+04

TABLE XII. NUMBER OF NEUTRONS LOST THROUGH VARIOUS SURFACES IN EACH PROBLEM

Incident Source	Problem*	$E_{incid.}$ (Mev)	Surface**								
			S1	S2	S3	S4	S5	Total Side	Front	Back	Total
30,000	Inner Grp 1	4.16	4	10	11	11	7	43	565	229	837
30,000	Inner Grp 2	2.07	-	1	1	4	-	6	611	5	622
20,000	Inner Grp 3	1.14	-	-	-	-	-	-	450	-	450
20,000	Inner Grp 4	0.63	-	-	-	-	-	-	376	-	376
20,000	Inner Grp 5	0.23	-	-	-	-	-	-	211	-	211
20,000	Inner Grp 6	0.05	-	-	-	-	-	-	20	-	20
140,000	TOTAL INNER		4	11	12	15	7	49	2233	234	2516
30,000	Outer Grp 1	4.16	1075	1704	944	627	175	4525	563	216	5304
30,000	Outer Grp 2	2.07	1270	1417	479	180	22	3368	612	12	3992
20,000	Outer Grp 3	1.14	845	636	142	22	-	1645	413	-	2058
20,000	Outer Grp 4	0.63	873	334	30	2	-	1239	420	-	1659
20,000	Outer Grp 5	0.23	658	88	1	-	-	747	255	-	1002
20,000	Outer Grp 6	0.05	278	8	-	-	-	286	36	-	322
140,000	TOTAL OUTER		4999	4187	1596	831	197	11810	2299	228	14337
280,000	TOTAL INNER AND OUTER		5003	4198	1608	846	204	11859	4532	462	16853

*"Inner" neutrons impinged on the central portion of the tank face; "outer" neutrons were incident on the other portion.

**The total side surface was divided into five unequal portions by boundaries at 0, 8, 20, 32, 56, and 92 cm depth. Of these, S1 is nearest the reactor, S2 is next, etc.

TABLE XIII. NEUTRON ENERGY LOST THROUGH VARIOUS SURFACES IN EACH PROBLEM (Mev)

Incident Mev	Problem*	$E_{incid.}$ (Mev)	Surface**								
			S1	S2	S3	S4	S5	Total Side	Front	Back	Total
124,600	Inner Grp 1	4.16	0.79	6.38	16.53	8.455	12.685	44.85	87.3	622.7	754.85
62,185	Inner Grp 2	2.07	-	0.58	0.21	3.0	-	3.80	47.3	4.0	55.1
22,879	Inner Grp 3	1.14	-	-	-	-	-	-	21.9	-	21.9
12,568	Inner Grp 4	0.63	-	-	-	-	-	-	12.4	-	12.4
4,512	Inner Grp 5	0.23	-	-	-	-	-	-	4.4	-	4.4
1,003	Inner Grp 6	0.05	-	-	-	-	-	-	0.25	-	0.25
227,747	TOTAL INNER		0.79	6.96	16.74	11.455	12.685	48.65	173.55	626.7	848.90
124,750	Outer Grp 1	4.16	1156.4	2094.2	1284.6	887.0	301.4	5723.7	82.5	667.5	6473.7
62,233	Outer Grp 2	2.07	707.0	937.1	332.8	109.7	9.7	2096.3	54.9	16.9	2168.1
22,890	Outer Grp 3	1.14	269.0	217.1	57.3	9.3	-	552.8	23.5	-	576.3
12,506	Outer Grp 4	0.63	160.5	70.6	7.0	0.5	-	238.6	14.6	-	253.2
4,530	Outer Grp 5	0.23	51.9	7.2	0.3	-	-	59.3	5.0	-	64.3
1,000	Outer Grp 6	0.05	7.5	0.3	-	-	-	7.8	0.5	-	8.3
227,909	TOTAL OUTER		2352.3	3326.5	1682.0	1006.5	311.1	8678.5	181.0	684.4	9543.9
455,656	TOTAL INNER AND OUTER		2353.1	3333.5	1698.7	1018.0	323.8	8727.2	354.6	1311.1	10392.8

*"Inner" neutrons impinged on the central portion of the tank face; "outer" neutrons were incident on the other portion.

**The total side surface was divided into five unequal portions by boundaries at 0, 8, 20, 32, 56, and 92 cm depth of these, S1 is nearest the reactor, S2 is next, etc.

TABLE XIV. NEUTRON COLLISIONS TO CUTOFF OR ESCAPE IN EACH PROBLEM

Histories	Problem*	$\bar{E}_{incid.}$ (Mev)	Collisions to Cutoff: Total Cutoffs	Collisions to Cutoff: Total Collisions	Collisions to Cutoff: Collisions per Cutoff	Collisions to Escape: Total Escapes	Collisions to Escape: Total Collisions	Collisions to Escape: Collisions per Escape	Collisions to Escape: $\bar{E}$ at Escape (Mev)
30,000	Inner Grp 1	4.16	29,163	203,290	6.97	837	3370	4.03	0.902
30,000	Inner Grp 2	2.07	29,378	185,140	6.30	622	2734	4.40	0.089
20,000	Inner Grp 3	1.14	19,550	111,490	5.70	450	1928	4.28	0.049
20,000	Inner Grp 4	0.63	19,624	100,470	5.12	376	1458	3.88	0.032
20,000	Inner Grp 5	0.23	19,789	79,897	4.04	211	788	3.73	0.021
20,000	Inner Grp 6	0.05	19,980	49,468	2.48	20	74	3.70	0.013
140,000	TOTAL INNER		137,484	729,755	5.31	2516	10352	4.11	0.337
30,000	Outer Grp 1	4.16	24,696	168,280	6.81	5304	15,036	2.83	1.221
30,000	Outer Grp 2	2.07	26,008	160,880	6.19	3992	11,454	2.87	0.543
20,000	Outer Grp 3	1.14	17,942	101,030	5.63	2058	5,984	2.91	0.280
20,000	Outer Grp 4	0.63	18,341	92,132	5.02	1659	4,681	2.82	0.153
20,000	Outer Grp 5	0.23	18,998	75,610	3.98	1002	2,653	2.65	0.064
20,000	Outer Grp 6	0.05	19,678	48,645	2.47	322	616	1.91	0.026
140,000	TOTAL OUTER		125,663	646,577	5.15	14337	40,424	2.82	0.666
280,000	TOTAL INNER AND OUTER		263,147	1,376,332	5.23	16853	50,776	3.01	0.617

*"Inner" neutrons impinged on the central portion of the tank face; "outer" neutrons were incident on the other portion.

TABLE XV. PROBABLE NEUTRON CAPTURE RATES BY DEPTH AND RADIUS*

CM	0-30	30-45	45-60	60-75	75-90	90-105	105-	120.68-
0- 1	1.9758+12	1.7783+12	1.9123+12	1.8269+12	1.7846+12	1.8040+12	1.6780+12	
1- 2	2.1896+12	2.0616+12	2.0807+12	2.0574+12	1.9508+12	1.8681+12	1.6860+12	
2- 3	1.8668+12	1.8434+12	1.7725+12	1.8020+12	1.7038+12	1.6525+12	1.3748+12	
3- 4	1.5064+12	1.4341+12	1.5578+12	1.4149+12	1.3887+12	1.3367+12	1.0004+12	
4- 5	1.2526+12	1.2351+12	1.1700+12	1.1642+12	1.1327+12	1.0533+12	7.4055+11	
5- 6	9.8244+11	9.8025+11	9.4029+11	8.9062+11	8.7873+11	8.4296+11	5.9759+11	
6- 7	8.0218+11	7.5637+11	7.4351+11	7.7184+11	7.2836+11	6.9109+11	4.4571+11	
7- 8	6.0569+11	6.2707+11	6.2798+11	6.0913+11	5.5938+11	5.4352+11	3.8071+11	
8-10	4.8368+11	4.7833+11	4.5718+11	4.6929+11	4.4875+11	3.9874+11	2.6703+11	
10-12	3.4548+11	3.5840+11	3.5053+11	3.2652+11	3.2967+11	2.9215+11	1.8339+11	
12-14	2.6164+11	2.6303+11	2.7063+11	2.5151+11	2.4540+11	2.2593+11	1.4256+11	
14-16	2.2334+11	2.1980+11	2.0860+11	1.9767+11	1.9848+11	1.6766+11	1.1847+11	
16-18	1.6718+11	1.7386+11	1.6453+11	1.6559+11	1.6111+11	1.3710+11	8.8513+10	
18-20	1.5097+11	1.4136+11	1.3459+11	1.3077+11	1.3533+11	1.1502+11	6.8777+10	
20-22	1.1509+11	1.1663+11	1.1634+11	1.0874+11	1.0356+11	9.3186+10	5.5609+10	
22-24	9.8124+10	9.3438+10	9.8471+10	8.8042+10	8.4214+10	7.9403+10	4.9757+10	
24-26	8.3278+10	8.2011+10	8.0466+10	6.9788+10	7.2247+10	6.6243+10	3.9810+10	
26-28	6.5438+10	6.3605+10	6.4819+10	6.2460+10	5.8109+10	5.3129+10	3.1161+10	
28-30	5.4917+10	5.9374+10	5.4002+10	5.1519+10	5.2377+10	4.5628+10	2.8579+10	
30-32	4.6055+10	5.0023+10	4.6842+10	4.3002+10	4.3011+10	3.6654+10	2.2899+10	
32-36	4.1321+10	3.5975+10	3.4495+10	3.2683+10	3.2924+10	2.8001+10	1.7883+10	
36-40	2.3750+10	2.3919+10	2.5370+10	2.4474+10	2.1886+10	2.0880+10	1.2775+10	
40-44	2.1663+10	1.7616+10	1.6023+10	1.5935+10	1.6558+10	1.3035+10	9.7684+09	6.3589+09
44-48	1.1856+10	1.3763+10	1.2269+10	1.1955+10	1.1380+10	1.0347+10	7.0759+09	2.2534+09
48-52	9.6734+09	9.7333+09	8.9680+09	9.5854+09	7.4009+09	7.2991+09	5.2408+09	2.4098+09
52-56	7.5878+09	7.8034+09	6.9638+09	5.9893+09	6.3464+09	5.7264+09	3.9882+09	2.1635+09
56-62	3.9455+09	5.2929+09	4.9480+09	4.3597+09	3.8595+09	3.3093+09	2.5311+09	1.1709+09
62-68	3.0281+09	2.5848+09	2.3693+09	2.2941+09	2.4231+09	2.4221+09	1.7981+09	8.6214+08
68-74	1.4239+09	1.5392+09	1.9581+09	1.5370+09	2.0442+09	1.2540+09	1.1019+09	6.6763+08
74-80	7.3329+08	9.2931+08	1.1640+09	1.2189+09	1.3537+09	1.0079+09	6.9025+08	3.8330+08
80-86	1.0092+09	6.7626+08	6.8034+08	7.2431+08	7.5098+08	4.0987+08	4.4713+08	2.2793+08
86-92	6.4802+08	4.2693+08	4.1121+08	4.6024+08	5.0992+08	3.1309+08	3.2497+08	1.8300+08

*The data shown are total neutron cutoff rates (n/cc-sec) with the group 6 rate increased to allow for low-energy neutron contributions.